CYCLIC CREEP DEFORMATION OF Al-4.6 WT% Mg IN THE DYNAMIC STRAIN AGING TEMPERATURE RANGE

by

Peter W. Leach

A Thesis submitted to the Faculty and the Board of Trustees of the Colorado School of mines in partial fulfillment of the requirements for the degree of Master of Science, Metallurgical Engineering.

Signed: Peter W. Leach
Peter W. Leach

Approved: Glen Edwards
Glen R. Edwards
Thesis Adviser

William M. Mueller
William M. Mueller
Head, Department of
Metallurgical Engineering

Golden, Colorado

Date: Feb. 12, 1979

ABSTRACT

In this investigation, the relationship between solute-dislocation interaction and cyclic stress (tension-tension) creep acceleration (the ratio of steady state cyclic to static creep rates greater that 1) is determined. A method is presented for quantifying the drag stress due to solute-dislocation interactions. The drag stress is related at constant values of temperature to the creep rate ratio, generated from constant and cyclic stress creep test pairs. It is shown that cyclic stress creep acceleration is a maximum when the drag stress is a maximum. In addition there is a drag stress above which one sees cyclic creep acceleration and below which one sees cyclic creep retardation. This unique value of drag stress results from a combination of applied stress and temperature, both of which can be varied.

TABLE OF CONTENTS

LIST OF FIGURES AND TABLES

TABLES

ACKNOWLEDGEMENTS

Realizing that I could not have completed this project without guidance and advice, I wish to express my sincere appreciation to the faculty of the Department of Metallurgy at the Colorado School of Mines. In particular, I would like to thank Dr. G.R. Edwards for his advice and encouragement, Dr. D.K. Matlock for his inspiring curiosity and Dr. D.L. Olson for his spirited interest in science.

Finally, I express my appreciation to the Colorado School of Mines and the National Science Foundation for financial support during my graduate studies.

CHAPTER I

INTRODUCTION

In practical engineering applications, one often finds systems in which a material is subjected to fatigue stresses superimposed on creep stresses at any temperature. A good example is a turbine blade which operates at high temperatures and high centrifugal forces. Creep is an obvious problem, but, in addition, the different resonant vibrating frequencies produce a dynamic flutter load superimposed on the centrifugal creep force. This combination of forces could jeopardize the safe operation of the engine if the result is an accelerated cyclic creep rate. The problem is not strictly confined to high temperature applications. Cryogenic pressure vessels are at the other extreme of both temperature and frequency, but it is important to study the effect of load cycling on the deformation characteristics for such applications as well.

The problems related to creep under cyclic loading conditions have been studied for many years, but the mechanisms controlling cyclic creep deformation are not yet thoroughly understood. Of particular interest in this study is the effect of stress cycling on creep deformation in the dynamic strain aging (DSA) temperature range. This is just one of many variables to consider in the study of deformation mechanisms. Other variables are crystal structure, strengthening mechanisms, purity, type, amplitude, waveform, and frequency of applied cyclic stress and the method of analysis. Since there are many variables involved, it is difficult to compare the various studies on the basis of one variable. A brief discussion concerning these variables will preview a detailed review of the important and most recent publications pertaining to cyclic creep.

CRYSTAL STRUCTURE

Metals from each of the three crystal systems - fcc, bcc, and hpc - have been used to study the effects of cyclic loading on creep. The fcc systems appear to be the one most often studied. This may be because fcc metals are used for high as well as very low temperature cyclic loading applications. Since the slip systems and interstitial site sizes are different for each crystal structure, one might expect characteristic differences in cyclic creep. Andrade and Jollif, (1952), investigated the effect of only one or two stress reversals on the creep deformation resistance of lead and cadmium at room temperature ($0.5T_m$). No acceleration of creep was noted for the cadmium, which is hcp. For the lead, which fcc, the creep rate increased after both the first and second stress reversals. Unfortunately, sufficient evidence to support this work has not yet been presented.

STRENGTHENING MECHANISMS

Strengthening mechanisms are very important when considering the deformation processes of metals. Solid solutions, precipitates, composites, dislocations and grain boundaries are the primary strengtheners in metals. Composites will not be considered here because they have no relation to this study. The other four methods of strengthening will be discussed with emphasis on solid solution strengthening.

Grain Size

Although the grain size is constant in this study, one must realize that grain size is an important variable in creep studies. At high temperatures, (above $0.6T_m$), one mechanism which can control deformation is grain boundary sliding. Consequently, smaller grain sizes with larger surface area to volume ratios promote higher creep rates. On the other hand, Bradley, August and Matlock, (1977), found that the creep rate of pure aluminum at $0.43T_m$ increased with grain diameter raised to the third power. This may have been due to the high stress dependence of the stress/temperature combination used. Shetty and Meshi, (1975), found that the cyclic creep behaviors of polycrystals and single crystal pure aluminum samples were qualitatively similar. Therefore, cyclic softening and cyclic hardening were not grain boundary related phenomena at temperatures ranging from 78 to 295 K. MacEwen and Ramaswami, (1970), in studying dynamic strain aging (DSA) in Al-Mg single crystals, found different activation energies for vacancy migration in single cyrstal and polycrystalline specimens. Values of 57.8 kj/mol and 38.5 kj/mol were found for single crystal and polycrystalline samples, respectively. Brindley and Worthington, (1969), also found a grain size dependence in the activation energy for vacancy migration in Al-Mg polycrystals. The activation energy decreased with a decreasing grain size, and they rationalized the results in terms of a grain size dependent dislocation velocity. From the differences in activation energies, yield strengths, and creep rates due to grain size, one can see that grain size is an important parameter and strengthening mechanism to consider in cyclic creep investigations.

Precipitates

Precipitates are important for strengthening metals used at any temperature, but they are particularly important for strengthening in high temperature alloys. In static creep, the effect of precipitates is quite well understood, but that is not the case with cyclic creep. Most of the studies on cyclic or fatigue-enhanced creep have been done on precipitation strengthened alloys. The effect due only to precipitates is difficult to determine since some form of solid solution strengthening is always present. In this study, high purity Al-4.6 wt. % Mg is used. The phase diagram of Al-Mg indicates that at room temperature the solubility of Mg in Al is about 1 wt. %. Precipitation should be expected. Powell (1978), doing transmission electron microscopy on high purity Al-4.6 wt. % Mg, found no evidence of precipitates at magnifications up to ninety thousand times. Therefore, the effects of precipitates are not related to this study and will not be considered further.

Solid Solutions

Solid solution strengthening is the most important strengthening mechanism related to this study. It is of primary concern because Al-4.6 wt. % Mg is a solid solution alloy. Although most alloys studied for the effects of cyclic loading on creep have some form of precipitation strengthening, it is important to determine the effects due solely to solid solution strengthening before one can deduce the effects due to precipitates.

Both interstitial and substitutional solid solution alloys have been examined for the effects of cyclic loading on the creep rate. Interstitial solid solution alloys of Nb-O and Fe-C have been studied by Sheldon and Yeske (1978), and Shetty and Meshi (1977), respectively. These works will be considered in detail later. Substitutional solid solution alloys have also been studied. High purity Al-4.6 wt. % Mg was studied by Coutinho et al, (1976), Nam (1974), Knauss (1975), and Kirk (1977). Other alloys which exhibit DSA have been studied, but generally these alloys have precipitates as well. The concern in this investigation is the effect of solutes only on cyclic creep in the DSA temperature range of Al-4.6 wt. % Mg.

There are two theories for the mechanism of DSA. Cottrell (1953) has proposed that DSA results from the interaction between moving dislocations and diffusing solute atoms. Dislocations are pinned by the solute until the stress is sufficient to free the dislocation from its solute atmosphere. The result is a stress drop and a jerky stress strain curve. Since diffusion is thermally activated and dislocation velocity is controlled by the applied strain rate, DSA is temperature and strain rate dependent. Johnson and Gilman (1959), have proposed that jerky flow results from dislocation multiplication. Initially, dislocation sources begin operating and generating many mobile dislocations, resulting in a drop in stress. The dislocations become immobilized at obstacles and tangles by the effect of solute pinning, and the stress begins to rise, repeating the process. While this theory explains the jerky flow, it does not describe the temperature and strain rate dependence of DSA. Figure 1 shows how the drag stress, a measure of solute-dislocation interactions, varies with temperature, strain rate and dislocation velocity (Cottrell and Jawson, 1949).

Dislocations

Dislocations and substructure comprised of ordered arrays of dislocations are important in the strength and deformation during creep of metals. Dislocation density, stacking fault energy, and subgrain formation are methods by which dislocations affect creep of metals. Creep of Al-Mg at elevated temperatures is controlled by dislocation glide, Sherby and Burke

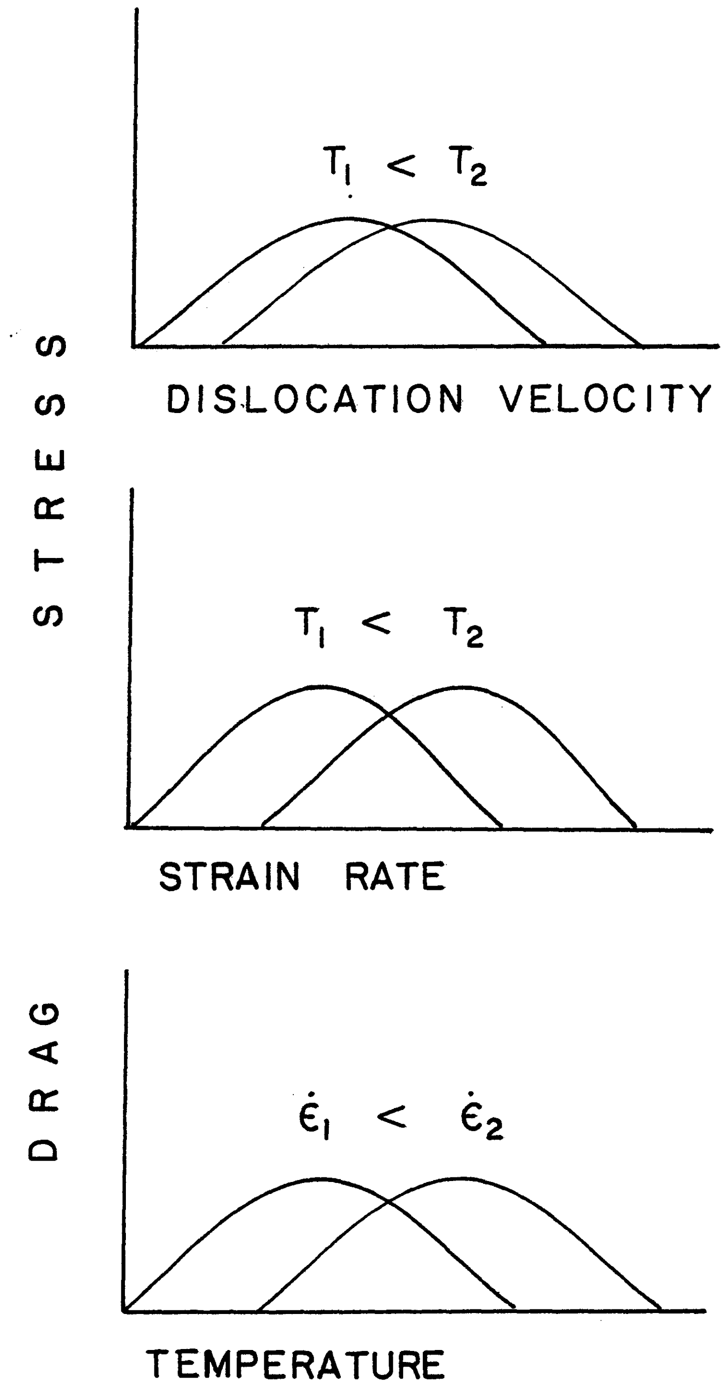

Figure 1 Schematic diagrams showing how drag stress varies with dislocation velocity, strain rate and temperature.

(1968). If dislocation glide is rate controlling, the creep rate should be proportional to the dislocation density. A sample first deformed at a high stress, which produces a high dislocation density, and then crept at a low stress, results in a faster creep rate than a sample originally crept at a low stress. The influence of stacking fault energy on creep deformation of metals where the rate controlling process is dislocation glide, is not yet completely understood. Suzuki locking and the effect of solutes on stacking fault energy are thought not to significantly influence the creep resistance. Sherby and Burke (1968) also reported that aluminum containing fine subgrains was stronger than that containing coarse subgrains.

One can imagine that by cycling the stress, the dislocation structure would be perturbed, and the rate of deformation could be affected. Powell (1978) did extensive TEM examination of dislocation structure in Al-4.6 wt. % Mg subjected to both constant and cyclic stress creep. He found that static loading resulted in a non-structured array of dislocations which included many jogs. Cycling the load caused dislocation loops to form, and the density of loops increased as the amplitude of unloading increased from 25% to 180%. The reader is referred to his work for a detailed discussion of the effect of stress cycling on dislocation structure.

PURITY

In a discussion about sharp yield points, Reed-Hill, (1973), addresses the problem of purity in an iron-carbon solid solution. How much carbon is necessary to pin the dislocations and cause a yield point? Assuming the dislocation density in soft annealed iron is 10^8 cm^{-2}, then in a 1-cm cube, there are 10^8 centimeters of dislocation. An iron atom in the bcc structure has a diameter of 2.5Å. In one centimeter, there are $4x10^7$ atomic distances. If there is one carbon atom for each iron along a dislocation, then there will be $4x10^7$ x 10^8, or $4x10^{15}$ carbon atoms. In a cubic centimeter, there are approximately 10^{23} iron atoms. The result is a ratio of 4 carbon atoms to 100 million iron atoms, or $4x10^{-8}$%. The significance of these calculations should be clear; very little solute is required to form dislocation atmospheres. One should keep this fact in mind when a discussion of the deformation of "pure" metals arises.

EXPERIMENTAL PARAMETERS

The material variables generally remain constant in an investigation of cyclic creep deformation characteristics. There are a few exceptions. For example, TRIP steels change crystal structure with plastic deformation, and with some alloys, investigators have felt that plastic strain induced precipitation of a second phase (Kennedy, 1962). Experimental variables, though, are usually widely varied, and as a result, comparison of the published investigations on cyclic creep is difficult. A number of these variables will be discussed to illustrate the complexity involved with making a detailed comparison of the published literature.

The type of applied cyclic stress is an important parameter. Variations and combinations of torsion, bending, tension and compression have been used to study cyclic creep deformation (Kitagawa, Jaske and Morrow, 1969; Reimann and Wood, 1964; Kirk, 1977, and Powell, 1978). Torsion is often applied along with an axial tensile load. As a result, a complex stress state which varies with the radius from the center of the test specimen is produced. This type of testing makes it difficult to determine an internal stress comparable to what is determined for simple uniaxial tension or compression. Bending has often been used as a means of cycling the load, and quite often it is used in combination with an axial load. Cycling by bending also results in a complex stress state which changes with the distance from the neutral axis of the beam.

Tension-tension and tension-compression are cycling methods which result in a simple uniaxial stress state. In applying tension-compression cycling, one must have a sample designed to prevent buckling. This is often done by making an hour-glass shaped sample, or a sample with a short gage length compared to the diameter. With these samples, the assumption of uniaxial stress is no longer valid. Unless the gage length is greater than twice the diameter (St. Venant's principle), the sample will experience a triaxial stress state and the results may be significantly affected.

The wave form used to apply the load for cycling is another important variable. Trapezoidal, triangular and sinusoidal waveforms are the ones most often used, (Kirk, 1977; Sheldon and Yeske, 1978; Kennedy, 1956). Results could differ considerably between tests with different waveforms used to apply the load. Whereas a cyclic creep test with trapezoidal loading may exhibit cyclic creep acceleration, the same test with triangular loading imposed may show cyclic creep retardation. The difference could be due to the length of time spent at peak stress for each wave form. The tests with trapezoidal loading will see a peak stress for roughly half the cycle, while tests with triangle loading will see peak stress for an instant. Sinusoidal loading, being a smooth curve, will eliminate any effects due to overshoot, common at higher frequency trapezoidal and triangular load cycling. Also, the time at peak stress or the time above some critical stress of a sine wave is between those for trapezoidal and triangle waves. One can see that the choice of wave form certainly can affect results, and in addition, the different wave forms used make the various cyclic creep data difficult to compare.

Amplitude of the cyclic load and frequency are two additional variables one must consider in analyzing cyclic creep data. In this paper, amplitude will be defined as follows: Static loading is 0% unloading; cyclic loading from σ to 0 is 100% unloading; cyclic loading from $+\sigma$ to $-\sigma$ is 200% unloading. As an example, cycling from $+\sigma$ to $+0.3\sigma$ is 70% unloading. Cycling from $+\sigma$ to -0.3σ is 130% unloading. Frequency assumes its normal definition in Hz. Changing the amplitude will change the internal stress, and if the material is tested in a temperature range of high stress sensitivity, one might see a significant difference in results. Knauss, (1975), working with Al-4.6 wt.% Mg, found that the plastic strain per loading cycle ($\Delta\varepsilon_p$), was a moderate function of amplitude at amplitudes from about 20% to 100% unloading. Below 20% unloading, he found $\Delta\varepsilon_p$ to be a very sensitive function of amplitude. Changing frequency can also have a significant effect on the cyclic creep deformation. At very low frequencies, one might get complete recovery during the "off load" half of the cycle. The result would be a series of primary creep curves which, when added up, would total much more strain than a static test of the same duration. At very high frequencies (about 10^{-4} Hz), the deformation mechanism is involved with short range atomic rearrangements. Scheffler, (1972), found the creep rate to be a function of frequency in the range of 10 to 19 kHz.

Nonsymmetrical wave forms, such as long off-load times with short on-load times, have been used to study the deformation. Also, stepped wave forms have been used by some to study the effect of load stepping in a cyclic fashion on the creep rate. Kiyotsugu and Marin, (1964), studied both nonsymmetrical and stepped wave forms to compare with theoretical creep deformation calculations.

Material variables and experimental variables in themselves make a systematic study of the literature complex enough. To compound matters just a bit more, one must consider the methods used to analyze the results.

Working with an alternating stress in a tension-tension mode, one can compare static and cyclic creep data in a number of ways. Some investigators have compared static and cyclic creep rates where the mean cyclic stress was equal to the static stress (Scheffler, 1972). Others make the comparison when the peak cyclic stress is the same as the static stress (Kirk, 1977). In addition, some define the cyclic creep rate as the strain for "on-load" time divided by the time on-load, or half of the cycle time (Gibbons, Herd, McCartney and McLean, 1973). Others take the total strain divided by the total time (Shetty and Meshi, 1977), while some take the time-averaged steady state creep rate of a cyclic test (Powell, 1978). Oftentimes, investigators do not attempt to analyze results in stage II or steady state creep (Sheldon and Yeske, 1978; Shetty and Meshi, 1975). If this is true, one must guess what effect the changing structure of primary creep might have on the results. If acceleration of the cyclic creep rate during primary creep is seen, what can one expect to see when the material reaches steady state deformation? This type of question arises because there is no uniform method of analysis. With all of the other variables to consider, it could be difficult to make a reasonable guess as to how the creep rates would compare in the steady state, based on what was found during primary creep.

The foregoing information was presented to illustrate the complexity involved with trying to review the literature in a systematic manner. A detailed review of a few interesting publications will follow. The materials, experimental procedure, and methods of analysis are all different, and the reader will find that the preceding discussion of the variables involved will be helpful in comparing the different investigations.

LITERATURE REVIEW

Kennedy, (1956), conducted an interesting cyclic creep study on lead at room temperature. Sine wave tension-tension cycling at 300 Hz was applied, and the results were compared for conditions of the peak cyclic stress and the static stress equal. Greater creep strain in a given time was found for cyclic loading than for static loading. Consequently, the creep life was reduced. The accelerating effect on the creep rate was inconsistent with just a simple increase in the number of dislocations. Kennedy thought fatigue or load cycling increased the number of dislocations, but decreased the effect of obstacles by increasing the mobility of the dislocations. To accomplish this, the path traversed by jogged dislocations under alternating stress was much greater than with a static stress. As a result, more vacancies were generated and climb and polygonization proceeded more rapidly. In studying aluminum alloys, Kennedy, (1962), found that the activation energy for fatigue-activated creep was not significantly different from that for static creep. This means that if the energy for creep includes the energy of formation and motion of vacancies, then the activation energy for fatigue-activated creep includes the same. Later works are in disagreement with this finding, however. The reason might be due to the large amount of scatter Kennedy reported in his results.

Price (1967) studied polycrystalline zinc at 30 C. ($0.4T_m$), using a sinusoidal loading at 40 Hz. The static stress was the same as the mean stress of the cyclic tests, and the amplitude was varied. Price felt that many of the earlier cyclic creep data were taken during primary or transient creep, and he made a point to reach steady state creep in his tests before taking data and changing the mode. In testing, it was found that during steady state deformation, the cyclic creep rate never exceeded the static creep rate. The explanation did not consider the creation of point defects of oscillating dislocations. In steady state creep, the mechanisms of work hardening and recovery were in equilibrium. If a cyclic stress was then applied, instantaneous extension was observed. Creep occurred over a range of stress from the static or mean stress, σ_m, to the peak stress which is the mean stress plus the stress amplitude, $(\sigma_m + \sigma_a)$. This creep was transient. As work hardening occurred only stresses near $(\sigma_m + \sigma_a)$ caused creep, but the time at that effective stress was very short compared with the time of the cycle. Steady state, then, depended on the stress dependence of creep and time spent in the effective stress region. In conclusion, creep fatigue in Zn at 30 C. took place against a background of thermal recovery with forward creep at stresses near the maximum only.

Kamel and Bessa, (1971), also studied the fatigue creep behavior of zinc. A static tensile load with alternating torsion was imposed. As the amplitude was increased from zero, the creep rate first decreased and then increased. The minimum in the curve was sensitive to both temperature and grain size. At a high temperature, the minimum was at a lower amplitude. For coarse grain samples, the minimum was sharper and occurred at smaller values of amplitude. Also, as the frequency of cycling was increased, the minimum became sharper and occurred at smaller amplitudes.

Kamel and Bessa felt that the minimum in the creep rate vs. amplitude curve was attributed to the possibility of a strain hardening effect resulting from a complex stress state. The motion of jogged screw dislocations created vacancies which initially pinned dislocations. By increasing the amplitude, the dislocations overcame the vacancy pinning, and also vacancies were pumped through dislocation cores to annihilation sites, permitting dislocation climb and increased creep rates. They did not adequately explain the temperature, grain size, and frequency effect on the creep rate. Unfortunately, this work cannot easily be compared with that of Price (1967).

Reimann and Wood, (1964), ran tests on iron which were similar to those of Kamel and Bessa, (1971). Iron was tested under conditions of axial tension with alternating torsion of 1,500 rpm at room temperature, ($0.2T_m$). Accelerated deformation was seen when cycling was initiated, but all tests failed in less than two hours, implying fatigue failure rather than stable creep deformation to failure. It was felt that cyclic straining acted as an injector of mobile dislocations. The applied axial load caused longitudinal drift and an increased rate of deformation. Because the samples failed so quickly under the moderately high frequency and relatively high strain (2, 3, and 4 degrees of twist), one would have difficulty in calling this a fatigue enhanced creep test rather than a complex stress state fatigue test.

Jakowluk, (1970), studied the effect of frequency and amplitude changes on the cyclic creep of an Al-Mg-Si alloy. Tests were run at 296 K in uniaxial tension with sine wave cycling. If the static stress equaled the peak cyclic stress, then cyclic creep was accelerated for a range of stresses. When the frequency was increased from 0.0033 Hz to 0.37 Hz, the cyclic creep rate increased and was always greater than the static creep rate. If the maximum cyclic stress was held constant and the mean stress and amplitude varied, results indicated that there was an optimum amplitude stress for cyclic acceleration, and cyclic retardation was observed above that amplitude. Tests were run holding the mean stress constant, and the same result with respect to amplitude was found.

Koterazawa, (1971), studied tensile creep of three different metals and found a transition in which the strain rate decreased rapidly as the period of cycling decreased. A curve of his data for titanium is given in Figure 2. When the strain rate ratio vs. the creep strain increment in one load-on period was plotted, all of the materials examined followed the same basic trend of transition, independent of stress and temperature. What resulted was a critical value of creep strain during one load-on period common to different materials, below which a rapid decrease in strain rate occurred. The transition appeared in fcc, bcc, and hcp structures, in both single and multi phase, with and without precipitation hardening; and in both substitutional and interstitial solid solutions. All the metals were of commercial purity (99% or less). In high purity metals, the transition was not apparent.

The transition was a result of creep strain recovery during the off-load portion of the cycle. For short periods, the creep strain increment was about equal to the recovery strain. The result was a very low strain rate. At long periods, recovery strains tended to be a limiting value, while the creep strain increased with longer periods. The result was an increasing creep rate with increasing period. The

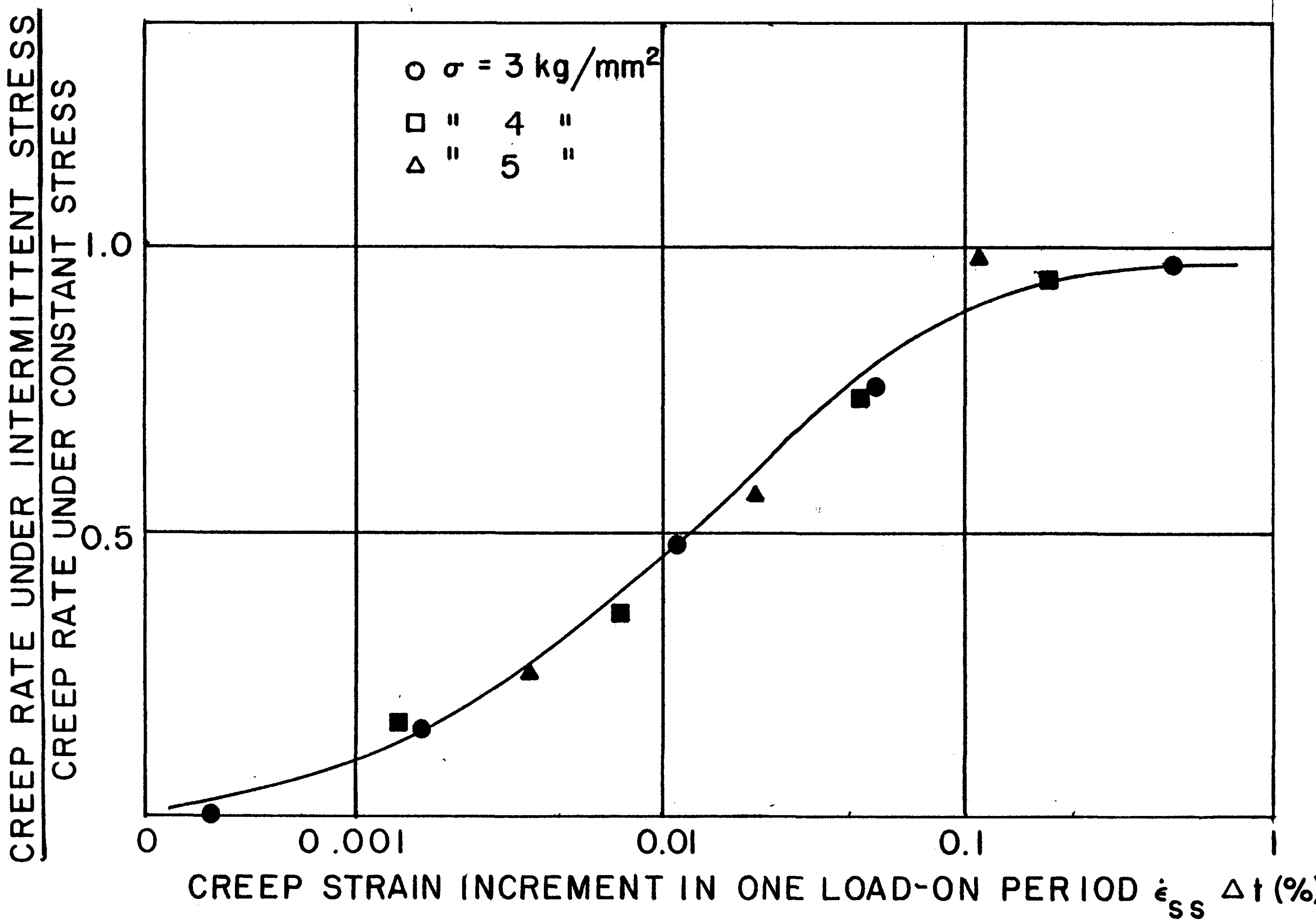

Figure 2 An example of the transition from a low creep rate ratio to a high ratio in titanium at 500 C., Koterazawa, 1971.

critical strain was really the limiting recovery strain.

Scheffler, (1972), studied two refractory metal alloys cycled at frequencies between 10 and 19 kHz in a tension-tension mode in the DSA temperature range of these alloys. In a molybdenum-based TZC (Ti, Zr, C) alloy, acceleration could be turned on and off instantaneously by applying and removing the dynamic drive. On reapplication of cycling, a large first stage extension was not observed. This implied that the mechanism for high frequency creep rate acceleration in TZC involved short range reversible atomic rearrangements rather than permanent long range diffusion-controlled structural alterations. Support for this idea was gained by noting that there was no change in microstructure. The acceleration in the TZC alloy was found to be a function of temperature and amplitude ratio (ratio of alternating stress to mean stress). The acceleration was greatest at the lowest test temperature and also increased with increasing amplitude ratio. The acceleration in the TZC alloy was also found to be frequency dependent, being greater at 19 kHz than at 15 or 10 kHz.

For T-111, a tantalum-based alloy, a change in static testing from a very low creep rate to a moderate creep rate was observed after testing for some time. This alloy depends upon solid solution strengthening for its high temperature properties. It was found that oxygen, as an interstitial, was lost during static testing at a high temperature and high vacuum. As a result, the creep rate increased. High frequency cycling was found to merely accelerate the deoxidation process in this alloy, and upon removal of the cycling, the creep rate either remained the same or very slightly decreased. Microstructural examination and post-test oxygen levels confirmed the deoxidation process.

Scheffler hypothesized that the high frequency strain rate acceleration was caused by a negative strain rate sensitivity. The flow stress decreased with increasing strain rate. In high frequency cycling, strain rates as high as 2,000 in./in. have been seen for a portion of each cycle. If the strain rate sensitivity is negative, then a transient decrease in flow stress is seen. A significant increase in strain rate during a portion of each cycle was observed, which resulted in a net increase in the measured strain rate.

Scheffler's paper was interesting in that it combined creep and fatigue in the temperature range of dynamic strain aging, but at very high frequencies. The results to be presented in this paper were obtained in the DSA range for Al-Mg at much lower frequencies and are quite comparable.

Shetty and Meshi, (1977), studied the influence of carbon on static and cyclic creep of alpha iron. The tests were run at room temperature in a tensile mode with 100% unloading of a trapezoidal wave and a two-minute period. The cyclic loading system was equipped with a spring and dashpot to eliminate the inertial effect of loading and unloading. Iron was purified with ZrH_2. Some samples were tested as purified, and others were carburized to 65 ppm carbon and quenched. A few samples were subsequently aged.

The purified iron showed cyclic creep acceleration at all stress levels examined, and the magnitude of acceleration did not appear to be related to the applied stress. The presence of carbon influenced the creep behavior of iron considerably. The cyclic creep was sensitive to both concentration and distribution of carbon, as evidenced by differences in the behavior of quenched iron and aged iron. Both quenched and quenched and aged samples showed greatly reduced static and cyclic creep rates compared with the purified iron. The aged samples exhibited almost no static creep, similar to the quenched iron, but showed considerable cyclic creep deformation, unlike the quenched sample. The acceleration was explained as follows: During cyclic creep, dislocations oscillate with a small fraction of this motion contributing to the observed cyclic strain. As a result of this oscillation, the average dislocation velocity will be considerably larger in cyclic creep than in static creep. The critical velocity of the carbon atoms required to cause dynamic pinning in static creep would not be adequate to cause pinning in cyclic creep. The difference in the cyclic creep behavior of the quenched samples and the aged samples was an interesting result. In the aged samples, most of the carbon atoms would be in precipitates. The fraction of atoms available for dynamic pinning would then be much smaller than in the quenched state. While the static creep rates were similar for the quenched samples and aged samples, the cyclic creep rates were much different, due to the amount of carbon free for pinning.

Sheldon and Yeske, (1978), studied another interstitial alloy, that of niobium-oxygen. The tests were conducted at temperatures of 295, 473, 673 and 873 K. These temperatures include the dynamic strain aging range for this alloy. Concentrations of 10, 100 and 1,000 wppm of oxygen in niobium were cycled at 0.13 Hz by a triangle wave form with 60% unloading. The stress was the same for all tests in the temperature range studied, and the data was analyzed in the first or primary stage of creep. The observations were as follows: 1) The total strain was the same for static and cyclic creep at all temperatures and concentrations. 2) In static tests, most of the strain was instantaneous, while for cyclic tests the same strain occurred over a number of cycles. 3) At temperatures and concentrations in which oxygen caused DSA in Nb, the cyclic strain rate was less than or equal to the static strain rate. 4) Only at 295 K was acceleration seen, and it was independent of concentration. At 873 K, it appeared that oxygen offered little restraint to deformation, and the ratio of cyclic to static strain rates for the 100 and 1,000 wppm alloys was 0.5 for each. It was felt that the observation of either acceleration or retardation under cyclic creep conditions was determined by a balance of three factors: (1) enhanced recovery through dislocation rearrangement and annihilation under cyclic stress; (2) reduced hardening due to suppression of solute atmosphere formation; and (3) a decrease in the average effective stress due to the lower average applied stress. It appeared that cyclic acceleration occurred only when the rate of atmosphere formation was sluggish. This may be suspect, but in light of the experimental method employed it is difficult to debate.

Kirk, (1977), studied an Al-4.6 wt. % Mg alloy and found cyclic creep acceleration in the temperature range of 318 to 357 K. He found that the increased frequency of Luder's band propagation during cyclic creep accounted for the accelerated cyclic creep rate. Enhanced recovery due to an excessive non-equilibrium concentration of vacancies generated during cyclic loading was thought responsible for the increased frequency of Luder's band propagation. Evidence was found to suggest that maximum creep acceleration was seen at a temperature of 338 K. This is also the temperature at which Borch, Shepard, and Dorn, (1960), and Rising, (1977), found that the activation energy for creep reached a maximum and was virtually indeterminate (see Figure 3). Because serrated yielding and Luder's band propagation were seen, it is felt that the solute-dislocation interaction had a large effect on the difference between the static and cyclic creep deformation of aluminum-magnesium.

This idea was further supported by the work of Nam, (1974), on the same Al-Mg alloy. He found cyclic creep

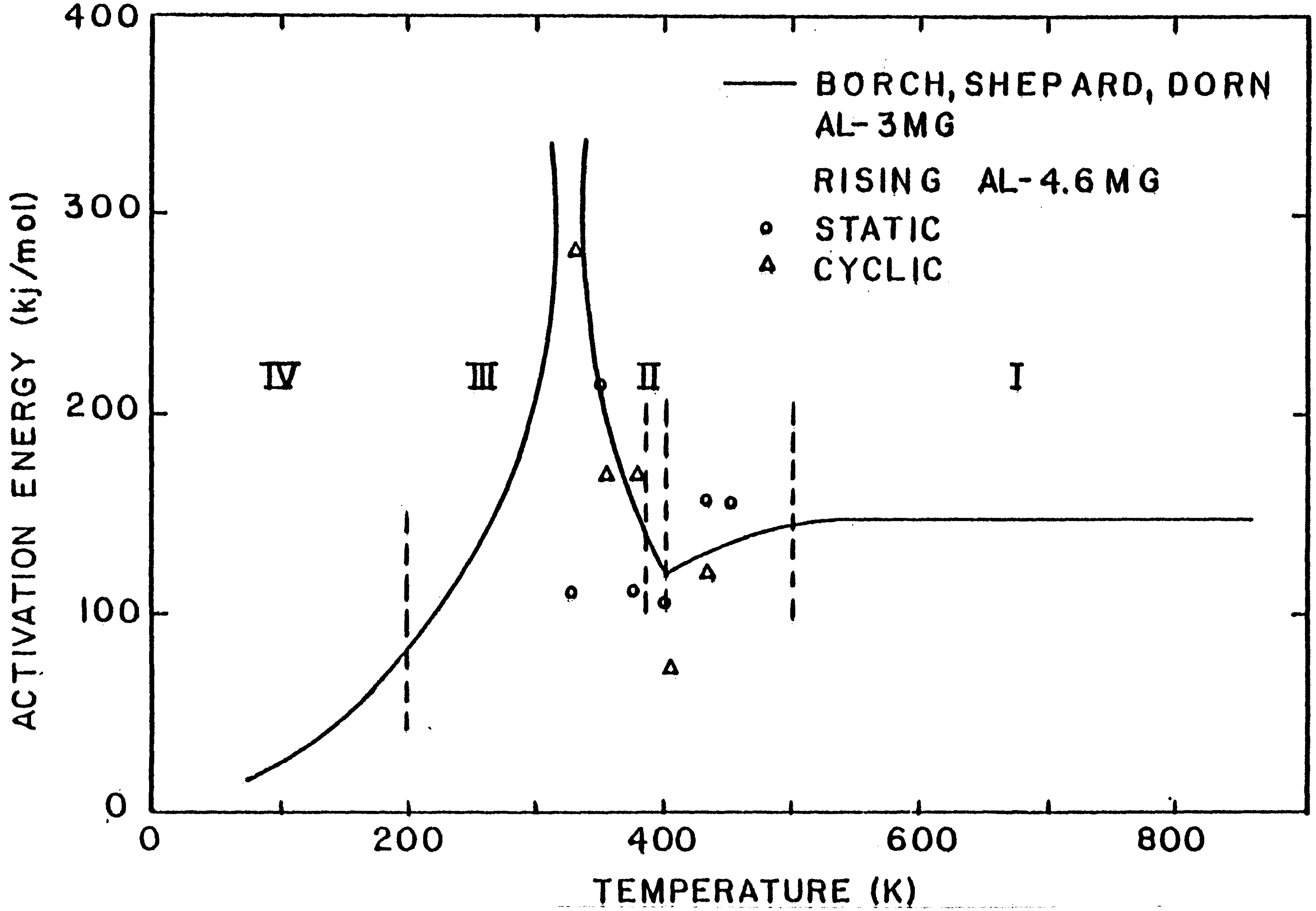

Figure 3 The apparent creep activation energy as a function of temperature for Al-3% Mg (after Borsch, Shepard and Dorn) and limited activation energy data for static and cyclic creep of Al-4.6 wt. % Mg (after Rising).

acceleration at temperatures below 423 K and retardation above that temperature ($0.45T_m$). Work by Sherby, Anderson and Dorn, (1951), indicated that DSA in Al-Mg alloys has an upper limit of temperature of about 423 K, depending on the strain rate of testing. This implies that the acceleration seen by both Kirk and Nam was related in some way to solute-dislocation interactions.

PURPOSE OF THIS INVESTIGATION

In cyclic creep testing, both acceleration and retardation of the creep rate compared with the static creep rate have been observed. Some investigators (Kirk, 1977; Nam, 1974; and Scheffler, 1972), have found evidence to suggest a direct correlation between cyclic creep acceleration and dynamic, solute-dislocation interactions. Further study of this correlation and of the stress dependence of cyclic stress creep acceleration on an Al-4.6 wt. % Mg alloy was the intent of this investigation. To accomplish this, compression tests were run at temperatures from 197 to 400 K to determine the stress sensitivity. From these data, the drag stress due to dynamic solute-pinning of dislocations was determined.

The drag stress was then related to the creep rate ratio (ratio of steady state cyclic to static creep rates) by running tensile static and cyclic creep tests in the temperature range from 197 to 485 K.

CHAPTER II

EXPERIMENTAL PROCEDURE

In this investigation, high purity Al-4.6 wt. % Mg was used. This alloy, made by Alcoa, was specifically prepared by vacuum casting 99.99% pure aluminum with proper additions of 99.99% pure magnesium. The material was then extruded into 1.9 cm diameter rods which were fully annealed. Chemical analysis showed the following: Less than 0.01 wt. % Si, Fe, Cu, Mn, Cr, Ni, Zn, Ti, Be; 4.61 wt. % Mg and the balance, Al.

Machined samples used in this investigation were of two types. Compression samples, nominally 6.35 mm diameter by 9.53 mm in length, and round reduced section tensile samples with a nominal gage length of 2.54 cm by 4.8 mm diameter were used. The machined samples were annealed in a Varian Marshall tube furnace (Model #1039) for 1.08 hours at 623 ± 2K. The anneal, conducted in a vacuum of 5×10^{-4} torr with air cooling, resulted in a uniform grain size of 0.249 mm.

Compression Tests

An MTS Model 810 electro-hydraulic closed loop testing system was used for the compression tests. Figure 4 illustrates the assembly used in conducting the compression tests. All of the tests were run in strain control using a ramp function. Load-displacement was continuously recorded using an MTS Model 632.11 extensometer ($\pm$ 15% on a one-inch gage length) and an MTS Model 661.21 A-01 load cell (5,000 pound

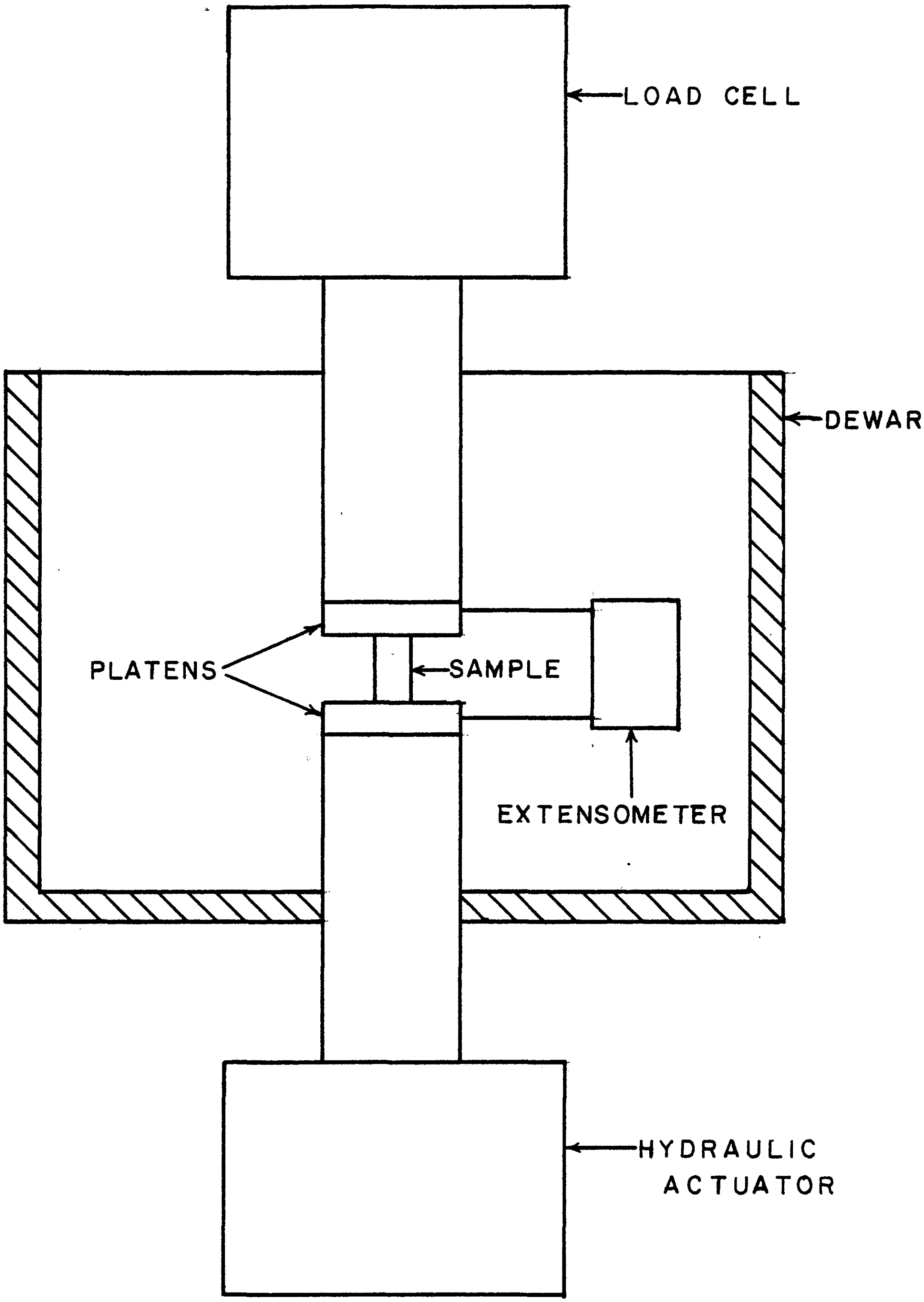

Figure 4 A schematic diagram of the compression test system used to generate flow stress-temperature data.

capacity). The recorder used was an MTS Model 431.21 X-Y recorder and the data was reduced from the recorded load displacement curves.

For test temperatures above 300 K, antifreeze, in a closed system, was heated in a Blue M constant temperature bath (Model #MW-1145-A1) and circulated through transfer coils immersed in transformer oil contained in the testing dewar. Circulation was thermostatically controlled, and the temperature could be maintained to ± 1 K. For tests run at 271 K, a refrigeration system with an antifreeze reservoir was used to cool the thermostatically controlled circulating antifreeze. A mixture of dry ice and methanol was used to maintain the temperature constant for tests conducted at 197 K. Teflon tape provided excellent lubrication between the sample and platens, and strains of over 40% were seen with no barreling.

Creep Tests

Constant stress creep tests, which included both cyclic and static loading, were conducted using an Andrade-Chalmers lever arm with a maximum mechanical advantage of 10 to 1. The arm was designed for use with an Al-4.6 wt. % Mg tensile sample having a nominal gage length of 2.54 cm. The effective gage length of these samples was found by Knauss (1975) and Kirk (1977) to be 3.05 cm. The parametric equations

$$x = \{a/(1 + b\theta)\} \times \{ \cos\theta + b\sin\theta/(1 + b\theta)\}$$

$$y = \{a/(1 + b\theta)\} \times \{ \sin\theta - b\cos\theta/(1 + b\theta)\}$$

where $a = r_o L_1/(L_. - R\theta_o)$ and $b = R/(L_o - R\theta_o)$

r_o = maximum load moment arm length (0.495 m)

L_o = initial effective gage length (3.0 cm)

R = the radius of load application (4.95 cm)

were used to develop the curve for the constant stress arm (Garofalo et al, 1962). A schematic of the constant stress system is given in Figure 5. A photograph of the actual system, which includes the balanced constant stress arm, frame, weight pans, gripping assembly, furnace, strain measurement system (LVDT), and pneumatic load cycling system, is given in Figure 6.

For all creep tests, strain was measured using a Schaevitz Engineering Linear Variable Differential Transformer, (LVDT), Type 500 HR, with a Schaevitz signal amplification unit, Model CAS-025. The LVDT displacement verses time was continuously recorded on a Leeds and Northrup Speedomax XL recorder.

Temperature above 300 K was controlled with a Leeds and Northrup Electromax III controller and a Varian Marshall tube furnace. Temperature was monitored at the sample and did not vary more than ± 1 K. For tests run at 273 K and 197 K, an insulated stainless steel dewar replaced the furnace. Temperature was maintained constant with a mixture of ice and water for 273 K and dry ice and methanol for 197 K.

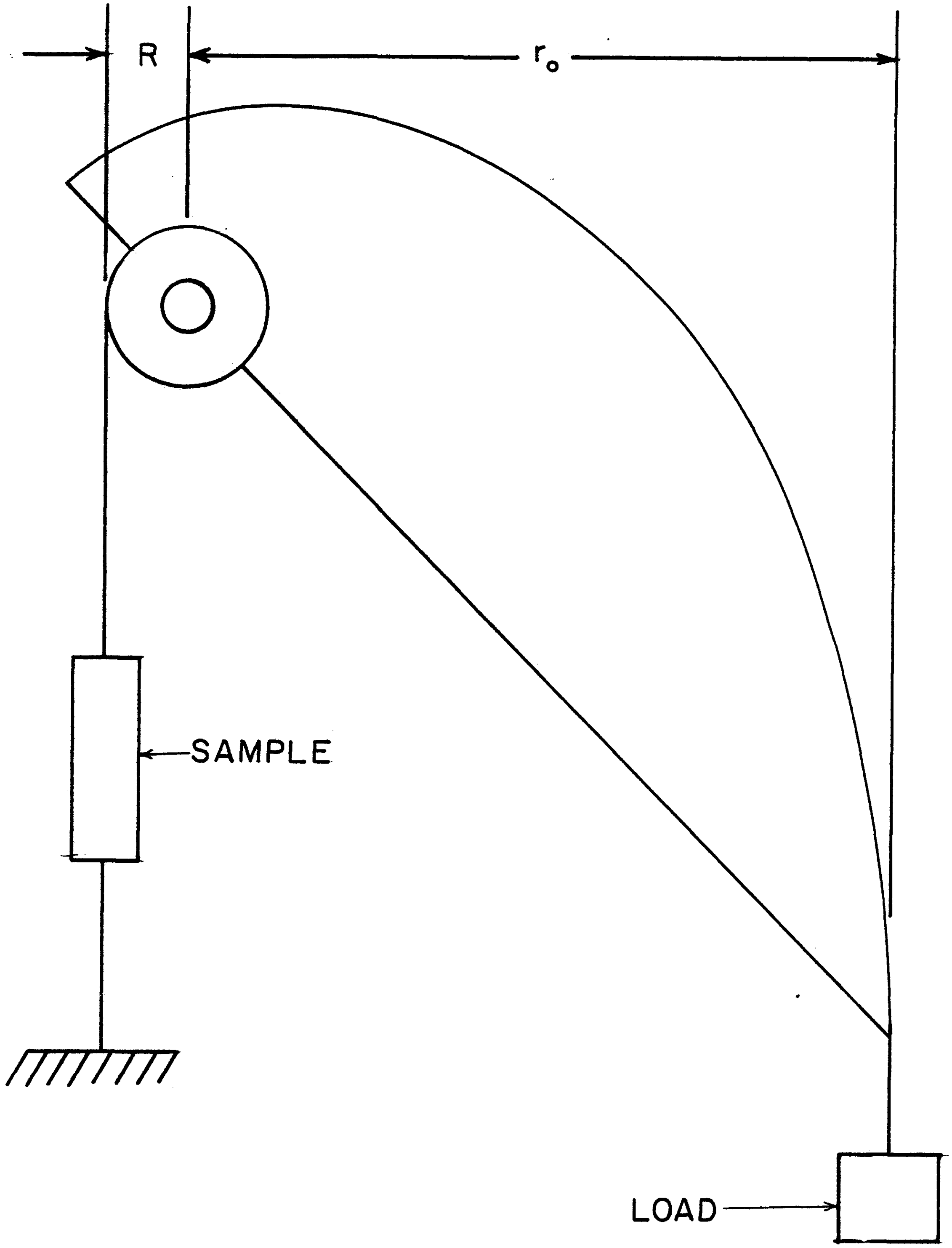

Figure 5 A schematic diagram of the Andrade-Chalmers constant stress lever.

Figure 6 A photograph of the constant stress creep system and the pneumatic lifting system used to cycle the load.

Cyclic loading was accomplished by means of a pneumatic lifting system which removed the lower of two weight pans. Cycling frequency for all tests was 0.0167 Hz with equal times on and off load.

A discussion of the design and building of the creep apparatus is given in Appendix I.

CHAPTER III

RESULTS AND DISCUSSION

A primary goal of this work was to study whether cyclic stress creep acceleration (the ratio of steady state cyclic to static creep rates greater than 1) was related directly to dynamic strain aging.

An investigation of two high temperature refractory metal alloys by Scheffler (1972) indicated cyclic creep acceleration was associated with dynamic strain aging. Both Kirk (1977) and Nam (1974) investigated an Al-4.6 wt.% Mg alloy and discovered that cyclic creep acceleration was related to solute-dislocation interactions or dynamic strain aging. The investigations by Scheffler (1972), Kirk (1977), and Nam (1974) provide sound support to the hypothesis that cyclic creep acceleration is related to dynamic, solute-dislocation interactions.

The intent of this investigation of Al-4.6 wt.% Mg was to build on the work of Kirk (1977) and Nam (1974). The complete temperature range and magnitude of solute-dislocation interactions were identified for strain rates of 10^{-3}, 10^{-4}, 10^{-5} and 10^{-6} sec^{-1}. The magnitude of solute-dislocation interactions was then compared with the ratios of the steady state cyclic to static creep rates from tests performed at temperatures from 197 to 485 K. The results showed a direct correlation between cyclic creep acceleration (a ratio of steady state cyclic to static creep rates greater than 1) and the magnitude of solute dislocation interactions.

To determine the temperature range and magnitude of solute-dislocation interactions, the flow stress temperature curves were developed for temperatures from 77 to 750 K at strain rates of 10^{-3}, 10^{-4}, 10^{-5}, 10^{-5} and 10^{-6} sec^{-1}. Compression tests were performed to generate the data at temperatures from 197 to 400 K. Data for temperatures below 197 K and above 400 K were taken from an investigation of Al-Mg alloys conducted by Sherby, Anderson, and Dorn (1951). These data were adapted to conform with the experimental parameters used in the present investigation.

Cyclic and static creep test pairs were then performed at temperatures from 197 to 485 K. The ratio of the steady state cyclic creep rate to the steady state static creep rate was used as a measure of cyclic creep acceleration. A ratio greater than 1 indicated acceleration, while a ratio less than 1 indicated retardation of the cyclic creep rate. The ratio of creep rates was compared with the magnitude of solute-dislocation interactions and a direct correlation between large solute-dislocation interactions and cyclic creep acceleration was confirmed.

Compression tests on Al-4.6 wt.% Mg run at nominal strain rates of 10^{-3}, 10^{-4}, 10^{-5}, and 10^{-6} sec^{-1} were performed at temperatures of 197, 273, 298, 318, 336, 355, 375 and 400 K. These tests permitted control of deformation while load was monitored. The data for Figure 7, which is a plot of log strain rate vs. log flow stress at 25% true strain, was generated from the compression tests. It is obvious, considering

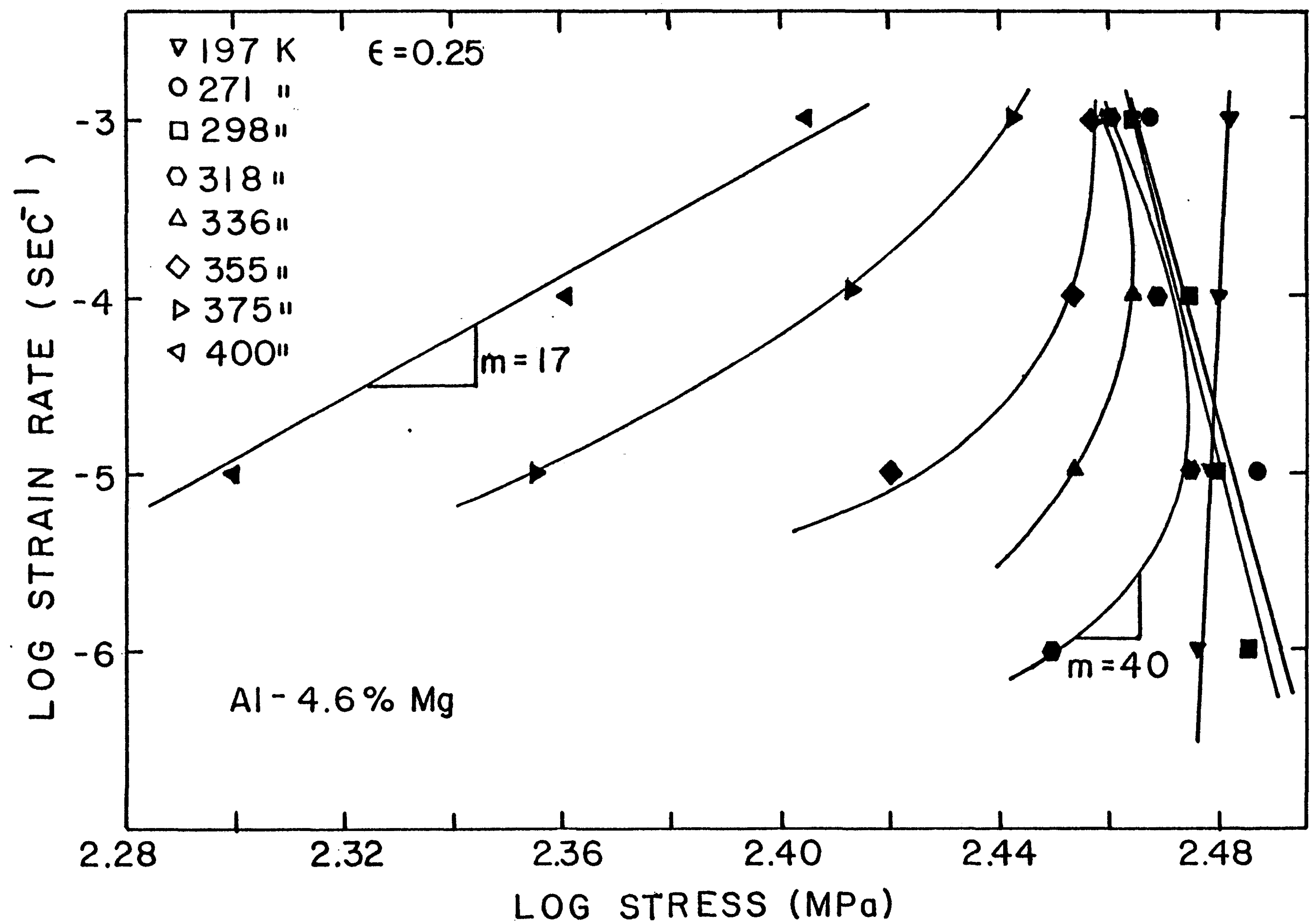

Figure 7 Curves of log σ vs. log $\dot{\varepsilon}$ from the compression data, showing the inverse strain rate sensitivity at temperatures of 271 and 298 K.

the near vertical lines in Figure 7, that an attempt to control the load and monitor the strain rate or deformation would have been virtually impossible. The inverse strain rate sensitivity (the negative sloped lines) of Figure 7 is also displayed in Figure 8, which shows flow stress vs. temperature at strain rates of 10^{-3}, 10^{-4}, 10^{-5} and 10^{-6} sec^{-1} and a true strain of 25% for Al-4.6 wt.% Mg. The temperature range over which inverse strain rate sensitivity was seen coincided with large solute-dislocation interactions as evidenced by the amplitude of serrations in the dynamic strain aging seen during testing. Figure 9 is a reproduction of an actual chart recording of load vs. deformation for Al-4.6 wt.% Mg tested at 271 K and a nominal strain rate of 10^{-6} sec^{-1}. Although individual serrations are not discernable in Figure 9, the amplitude of serrations can be obtained by measuring the width, in load, of the curve at any strain rate above the yield point.

Figure 10 is a plot of log strain rate vs. 1/T for Al-4.6 wt.% Mg. The data for each line of Figure 10 were taken at constant stress values from Figure 8 (shown as dashed lines in Figure 8). Assuming that deformation in Al-4.6 wt.% Mg can be represented by the equation $\dot{\varepsilon} = A \exp(^{-Q}/RT)$ where $\dot{\varepsilon}$ is the strain rate, A is a constant, Q is the activation energy, R is the gas constant and T is the absolute temperature, then from the slope of the lines in Figure 10, the activation energy, Q, can be determined. This was done and the value of Q for each line is shown in Figure 10. The activation energy

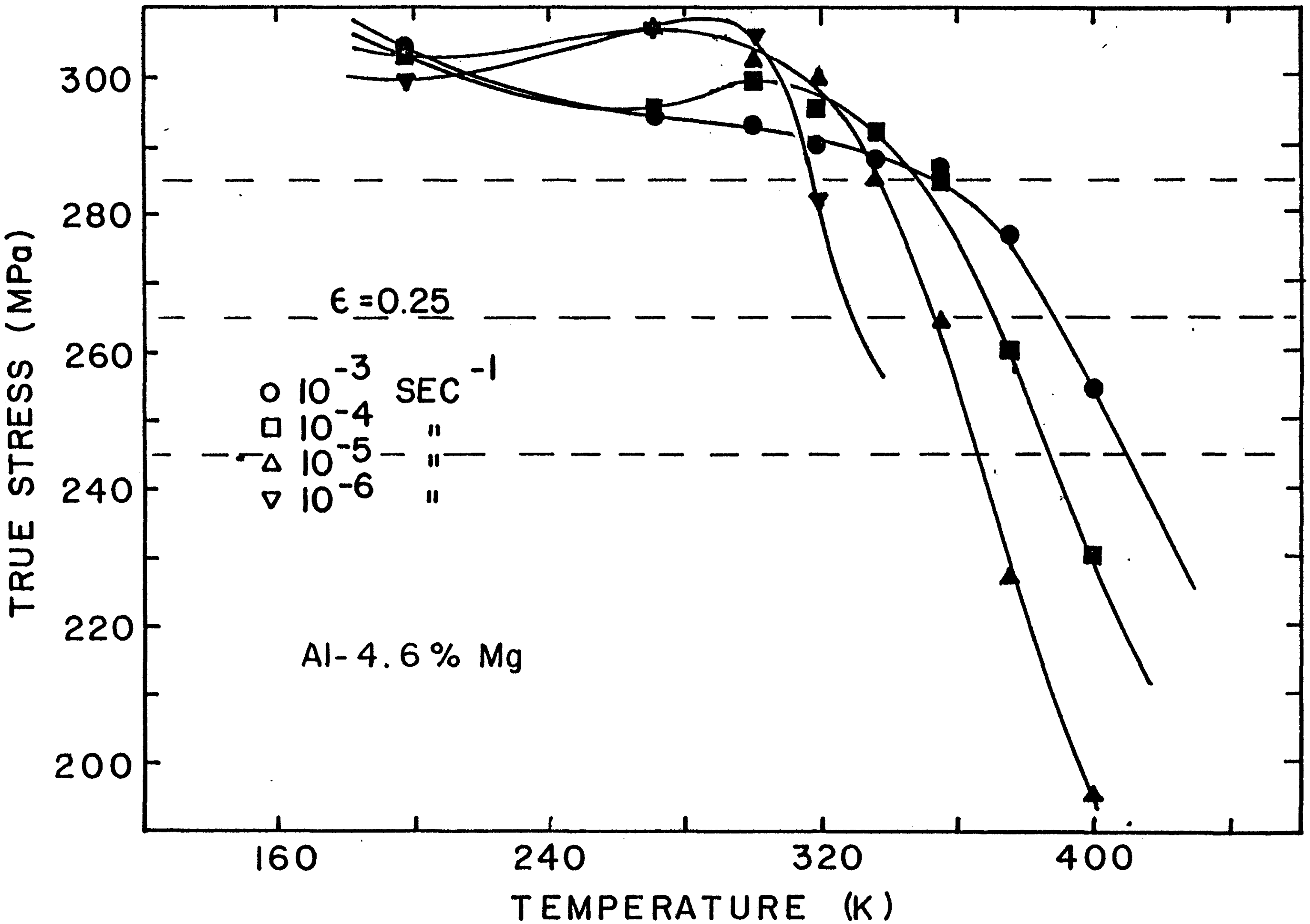

Figure 8 Flow stress vs. temperature curves for different strain rates showing the anomalous increase in flow stress with increasing temperature.

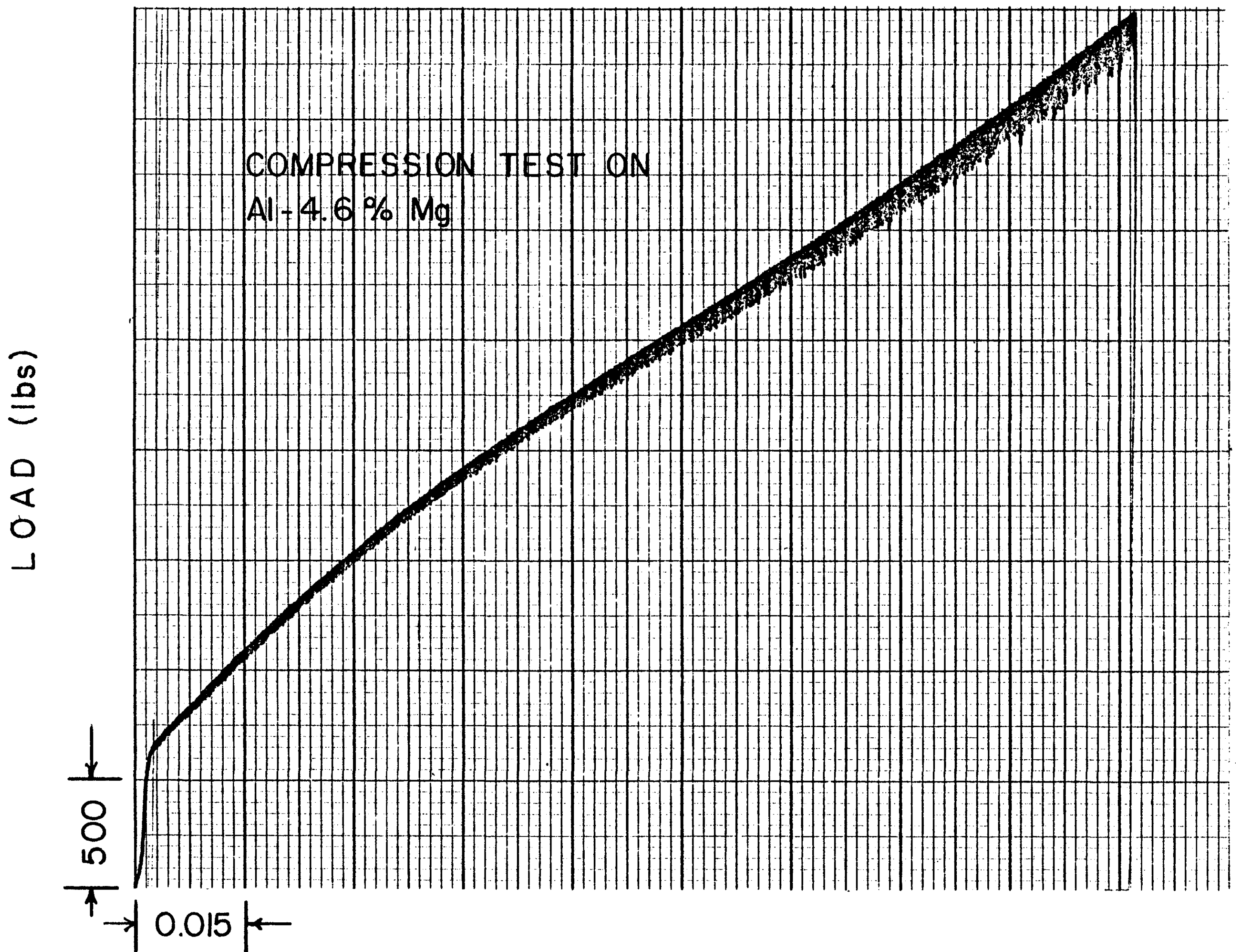

Figure 9 An actual load-deformation curve of Al-4.6 wt. % Mg at 338 K and 10^{-5} sec^{-1}. Note the serrated yielding.

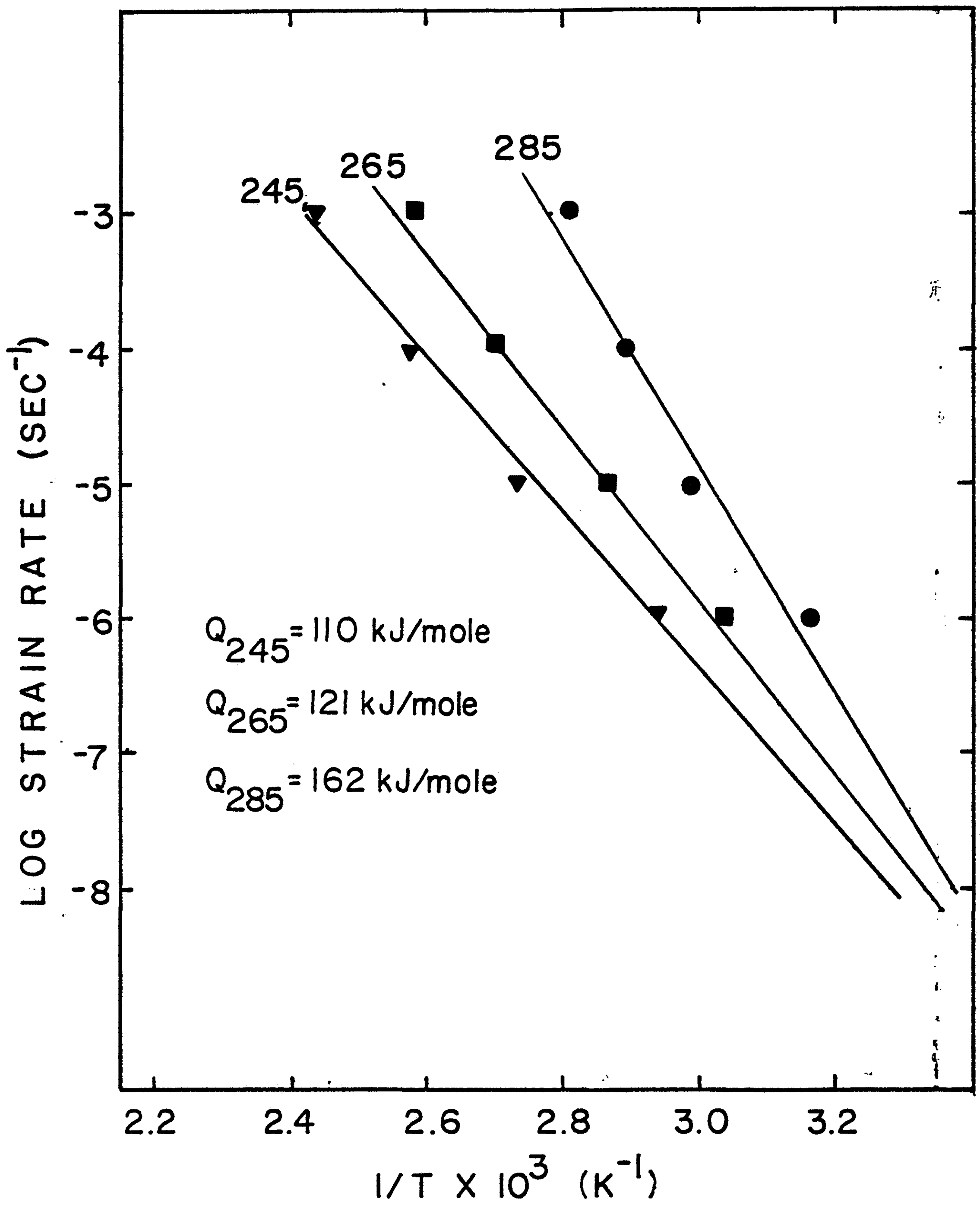

Figure 10 Log $\dot{\varepsilon}$ vs. 1/T at values of constant flow stress (MPa) to determine how the activation energy varies with flow stress.

can be seen to systematically decrease with a decrease in flow stress. This is not an unusual result for circumstances in which a decrease in flow stress removes the test environment further from the regime of maximum dynamic strain-aging. A similar result was found by Borch, Shephard and Dorn (1960) and Rising (1978) studying Al-Mg alloys. Their results are shown in Figure 2 where the activation energy was plotted vs. temperature. The activation energies determined from Figure 10 are at temperatures which fall on the high temperature side of the peak in Figure 2. The fan of curves in Figure 10 implies that the activation energy will approach anomalously high values as the stress is increased. This is similar to what is seen in Figure 2 as the temperature decreases. The high activation energy values coincide with strong solute-dislocation interactions seen as dynamic strain aging during compression tests. The relation, $\dot{\varepsilon} = A \exp(^{-Q}/RT)$, used to determine the activation energies, was used at a constant stress of under the assumption that the structure of the Al-Mg alloy remained constant during deformation. Considering that the degree of solute-dislocation interactions is a function of strain rate at a constant temperature, then the assumption of a constant structure is not valid. The activation energy varied with stress because the structure was not constant. If a method could be found to determine a constant structure in the temperature range of dynamic strain aging, then an activation energy for solute motion during dynamic strain aging could be determined. This idea will be addressed later in this chapter.

As was previously stated, the flow stress temperature curves of Figure 8 were extended by use of data from work by Sherby, Anderson, and Dorn (1951). They conducted tensile tests on aluminum-magnesium alloys with the magnesium content varying from zero to 3.1 at. % and at temperatures from 78 to 750 K. All of their tests were performed at a nominal strain rate of $2x10^{-3}$ sec^{-1}. Flow stress data to compare with the alloy of the present investigation (Al-5.1 atomic % Mg) were obtained by plotting flow stress vs. atomic % Mg from Sherby et al at a constant strain of 25% and temperatures of 78, 116, 422, 550, 650 and 750 K. The data from Sherby et al were extrapolated by a smooth curve out to 5.1 at % Mg to yield a value of flow stress for each of the temperatures 78, 116, 422, 550, 650, and 750 K. Figures 11, 12 and 13 are plots of flow stress vs. atomic % Mg. The points plotted represent data from Sherby, Anderson and Dorn (1951) and a smooth curve was then drawn through the points and extended to 5.1 at % Mg - the dashed line.

Since the flow stress values obtained from Figures 11, 12, and 13 were all for a strain rate of $2x10^{-3}$ sec^{-1}, they had to be adjusted for use at the different strain rates of the present investigation of 10^{-3}, 10^{-4}, 10^{-5} and 10^{-6} sec^{-1}. The adjustment was made as follows. For strain rates of 10^{-3} and 10^{-4} sec^{-1}, the flow stress values obtained by the

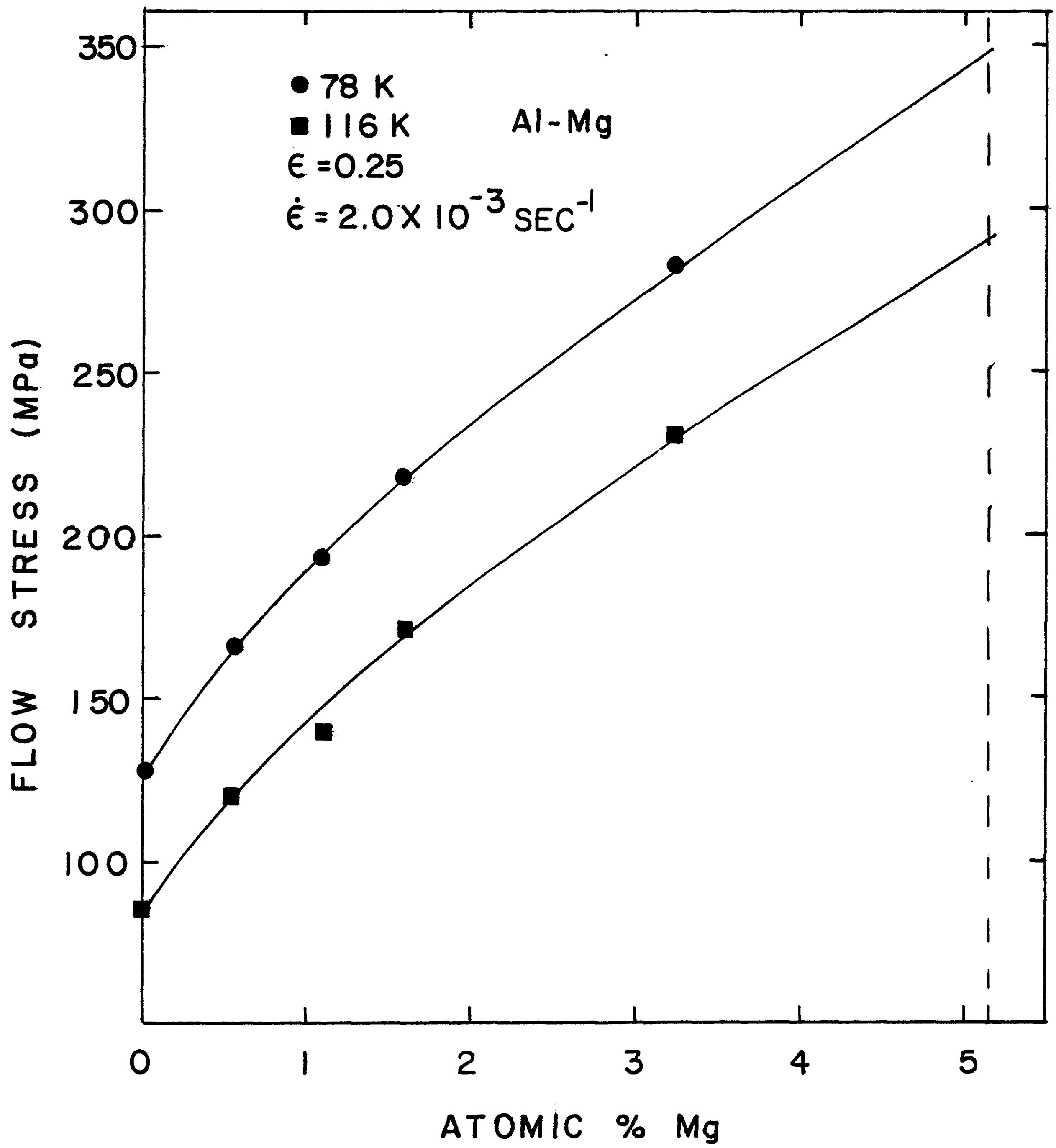

Figure 11 Flow stress vs. atomic percent Mg at 25% true strain for 78 and 116 K. The curves were extrapolated to obtain flow stress values at 5.1 at % Mg (from Sherby, Anderson and Dorn).

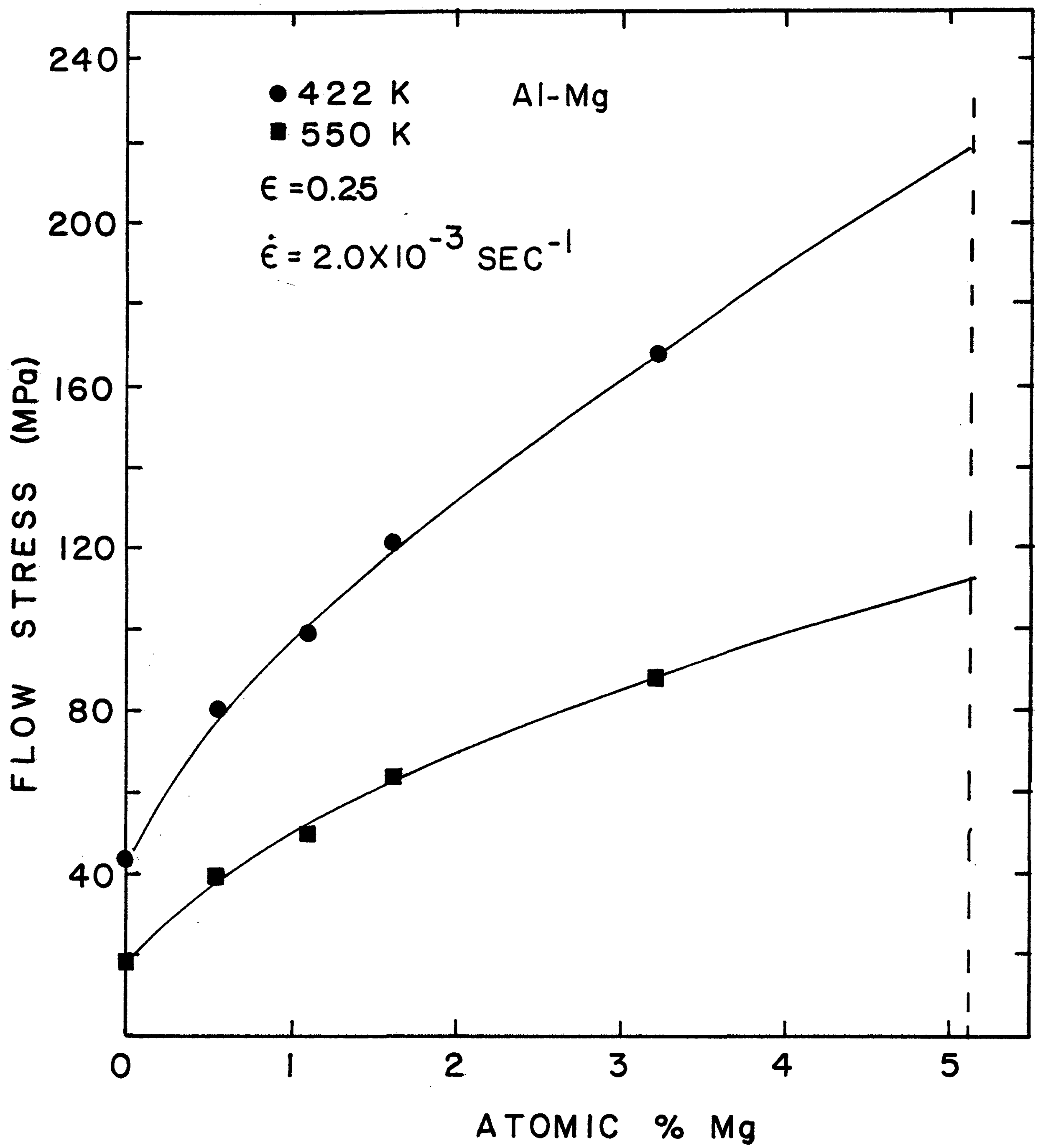

Figure 12 Flow stress vs. atomic percent Mg at 25% true strain for 422 and 550 K. The curves were extrapolated to obtain flow stress values at 5.1 at % Mg (from Sherby, Anderson and Dorn).

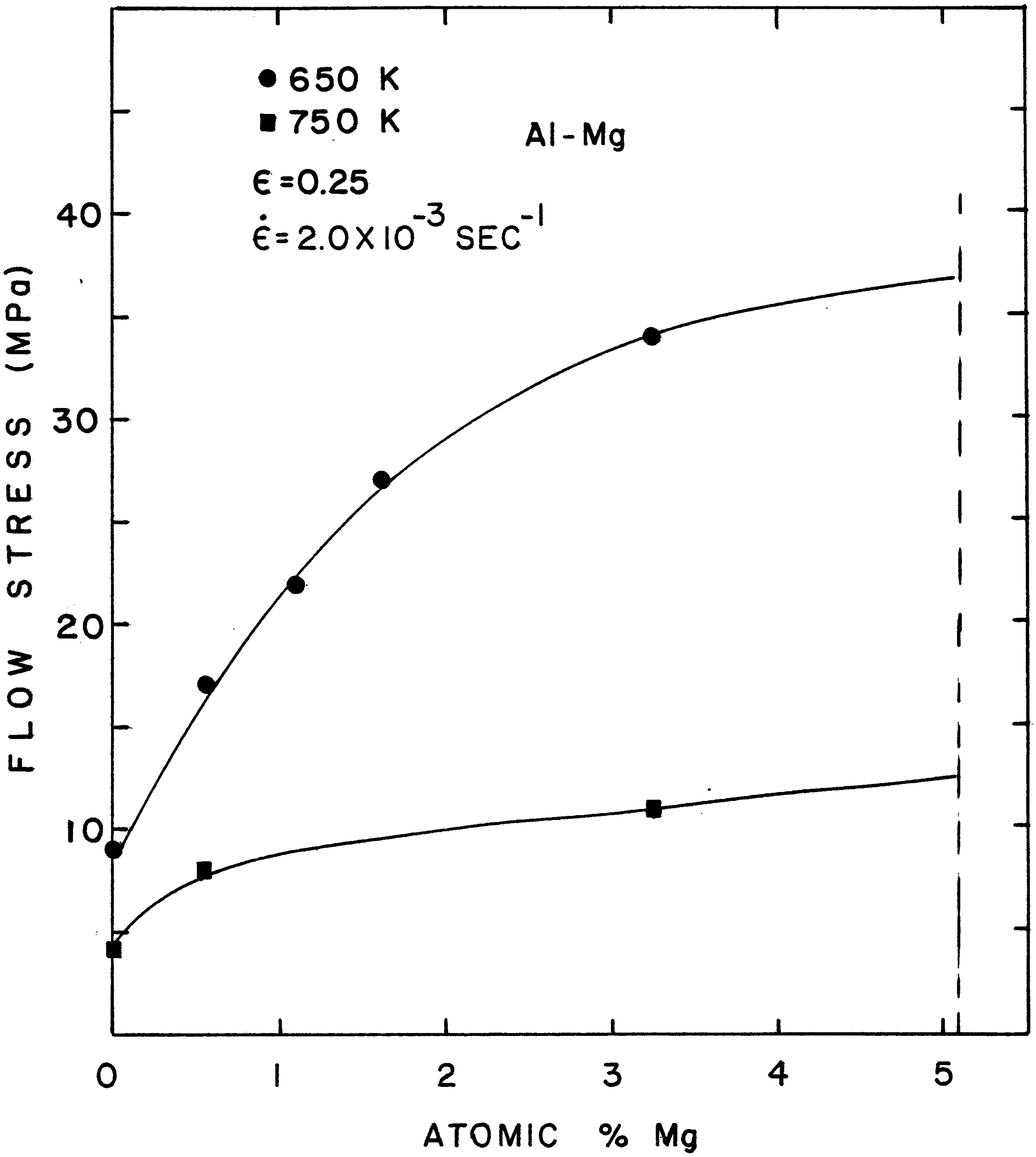

Figure 13 Flow stress vs. atomic percent Mg at 25% true strain for 650 and 750 K. The curves were extrapolated to obtain flow stress values at 5.1 at % Mg (from Shelby, Anderson and Dorn).

from the Sherby et al (1951) data were used as obtained by extrapolation. The completed flow stress vs. temperature curves for the strain rates of 10^{-3} and 10^{-4} sec^{-1} can be seen in Figures 14 and 15 respectively. For strain rates of 10^{-5} and 10^{-6} sec^{-1}, the flow stress was adjusted by use of the exponential relation $\dot{\varepsilon} = A\sigma^n$. By employing the appropriate value of n and using the flow stress values obtained from Figures 12 and 13 at temperatures of 422, 550, 650, and 750K, substitution into the relation, $\dot{\varepsilon} = A\sigma^n$ using $\dot{\varepsilon}$, the strain rate, equal to $2x10^{-3}sec^{-1}$, yielded values of the constant, A, for each temperature. Using the calculated values of A and the strain rates of 10^{-5} and 10^{-6} with the same appropriate values of n, flow stress values for the temperatures 422, 550, 650 and 750K were calculated. The calculated values are given in Table 1 and the extended flow stress vs. temperature curves for strain rates of 10^{-5} and 10^{-6} sec^{-1} are shown in Figures 16 and 17 respectively.

Flow stress curves which represent the strengthening of aluminum due to the solid solution of magnesium but exclude the strengthening due to dynamic solute-dislocation interactions have been drawn through the DSA range as dashed lines in Figures 14 through 17. The difference between the solid and dashed curves in Figures 14 through 17 represents a drag stress due to the dynamic solute pinning of dislocations. Figure 18, a plot of drag stress vs. temperature obtained from the difference between the solid and dashed lines in

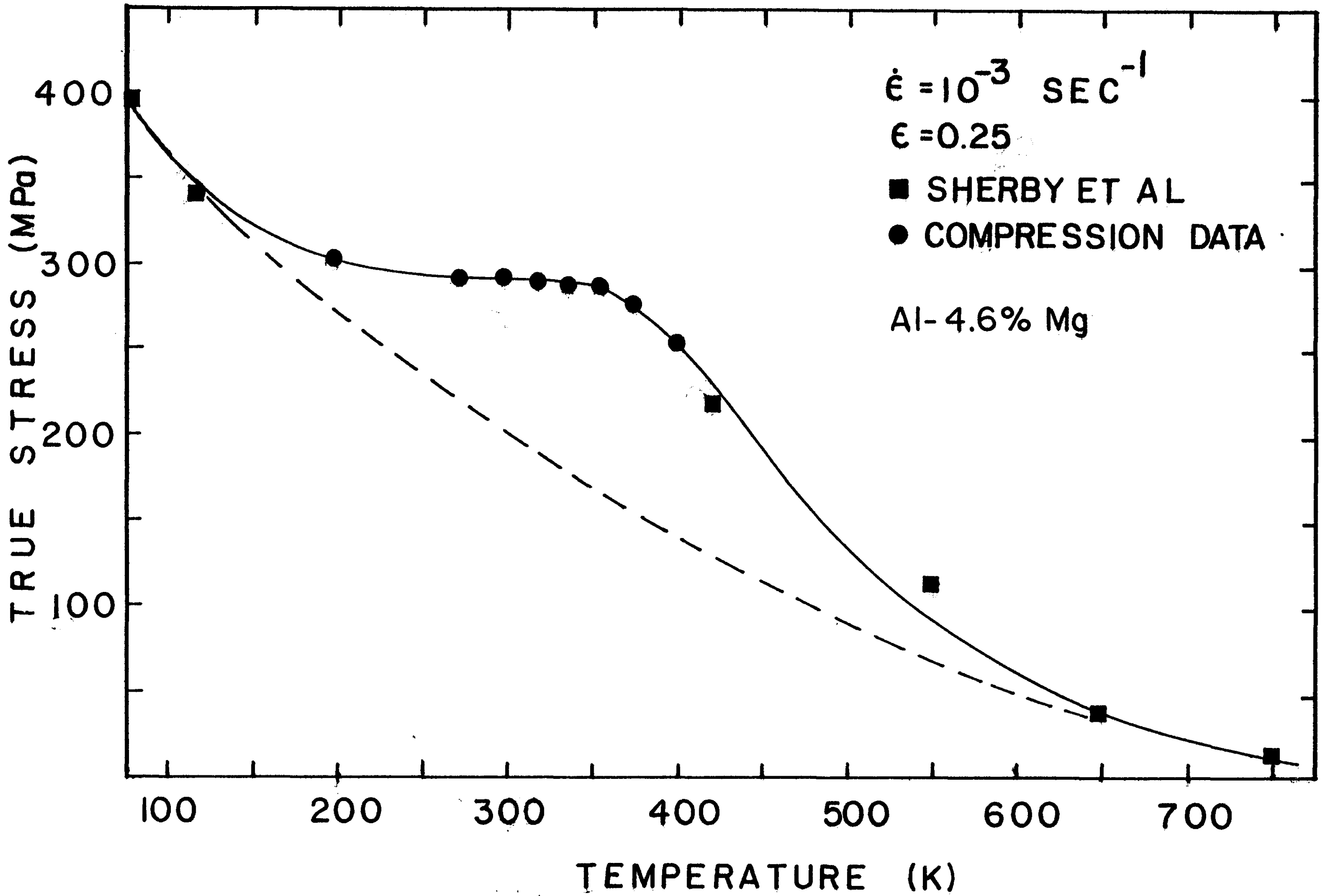

Figure 14 Flow stress-temperature curve extended at high and low temperature by the data from Sherby et al. The dashed line represents a theoretical flow stress-temperature curve of Al-4.6% Mg, but with no solute dislocation interaction.

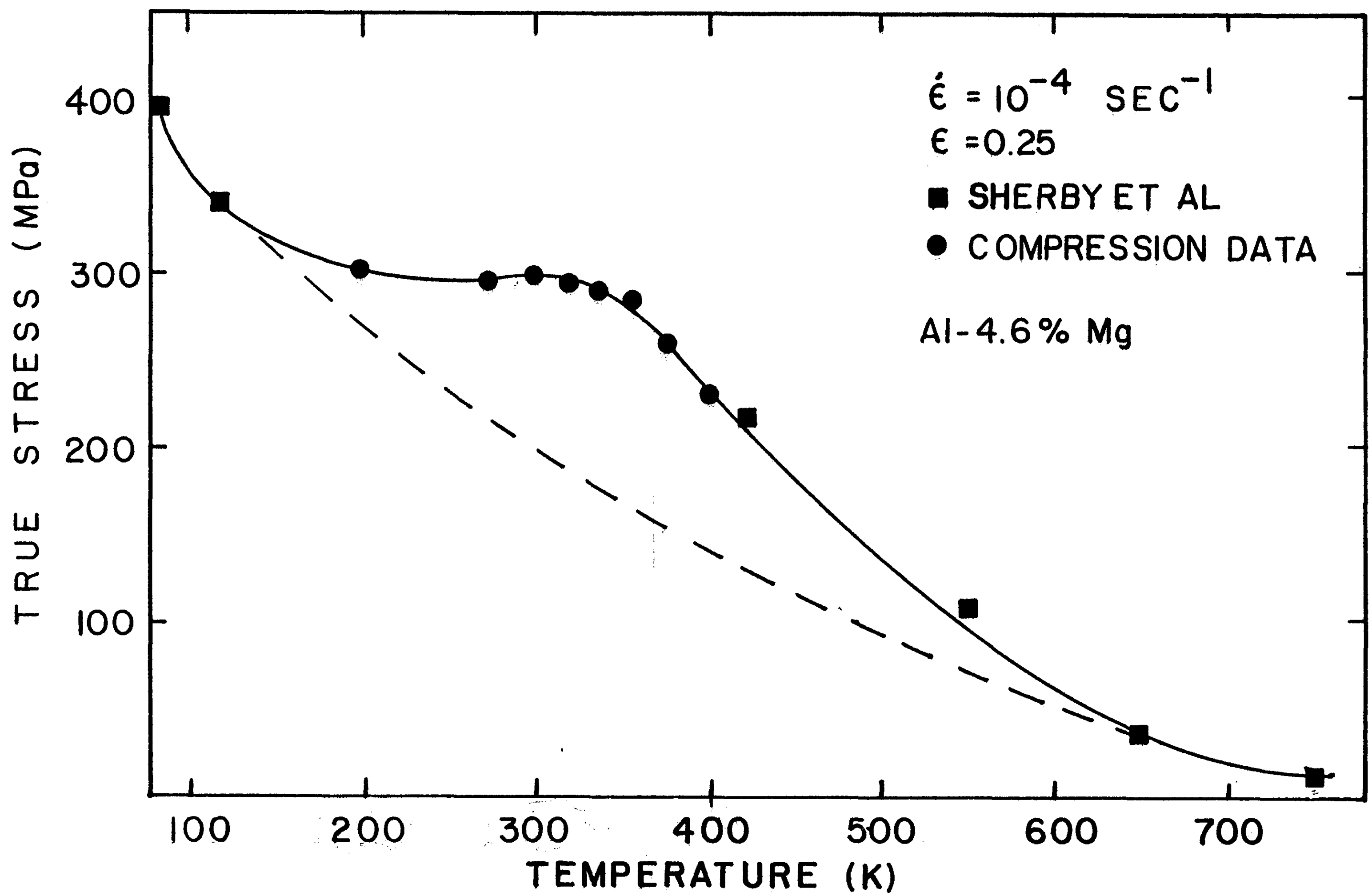

Figure 15 Flow stress-temperature curve extended at high and low temperature by the data from Sherby, et al. The dashed line represents a theoretical flow stress-temperature curve of Al-4.6% Mg, but with no solute dislocation interaction.

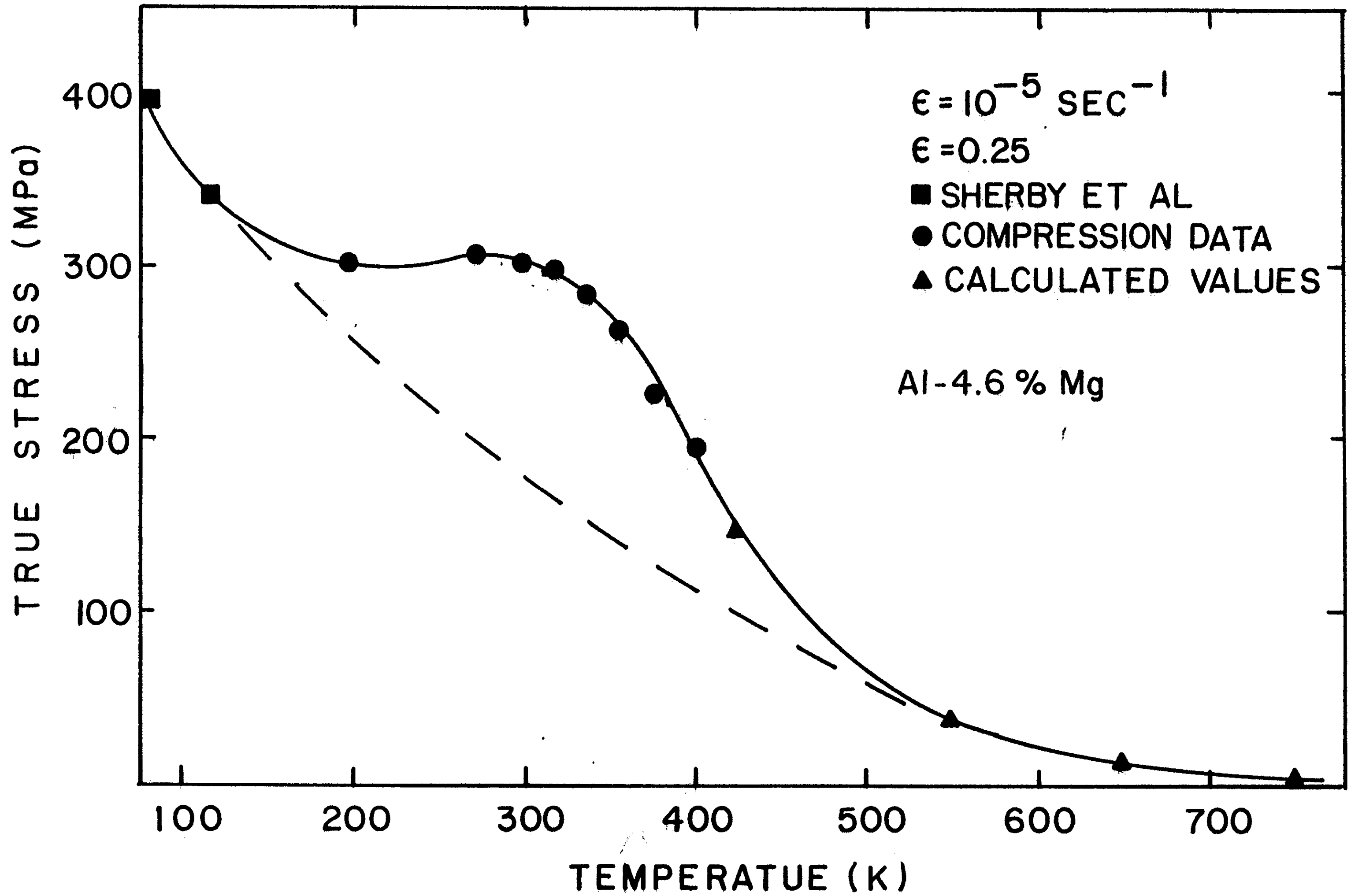

Figure 16 Flow stress-temperature curves extended at high and low temperatures by data from Sherby, et al, and calculations.

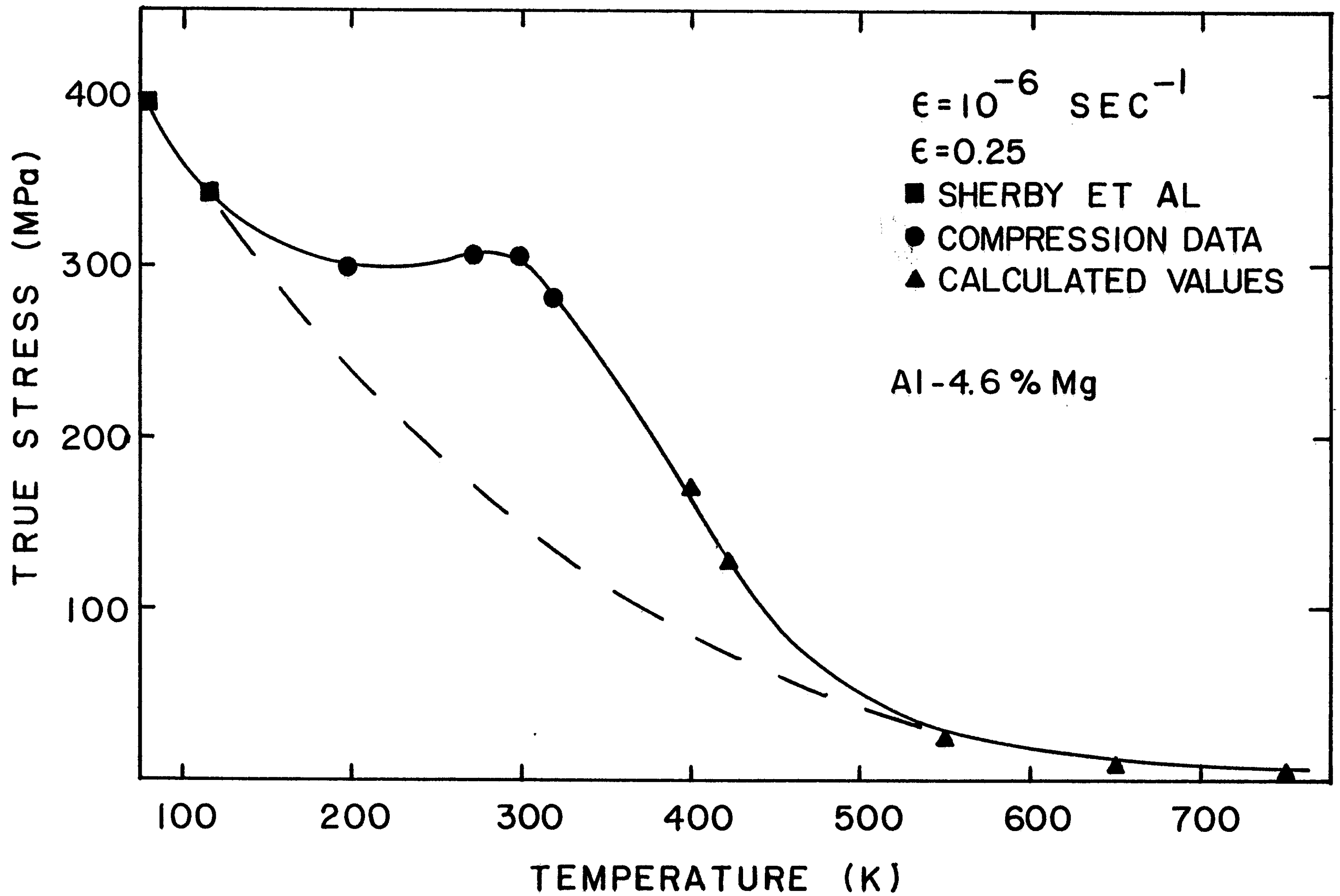

Figure 17 Flow stress-temperature curves extended from the relation $\dot{\varepsilon} = A\sigma^m$. The dashed line represents a theoretical flow stress-temperature curve of Al-4.6 wt. % Mg, but with no solute-dislocation interaction.

TABLE 1

Values of flow stress calculated from the expression $\dot{\varepsilon} = A\sigma^n$.

Temperature K	$\dot{\varepsilon}$ sec^{-1}	A	n	σ (MPa)
400	10^{-6}	55746	17	170
422	10^{-5}	340	14	149
	10^{-6}	340	14	127
550	10^{-5}	54758	5	38
	10^{-6}	54758	5	24
650	10^{-5}	19755	5	14
	10^{-6}	19755	5	9
750	10^{-5}	5892	5	4
	10^{-6}	5892	5	3

Figures 14 through 17, shows how the drag stress varies with temperature for any given strain rate. The temperature of the peak drag stress can be seen to increase with increasing strain rate. This finding is identical to what Cottrell and Jawson (1949) proposed, shown schematically in Figure 1.

In support of the drag stress illustrating solute-dislocation interactions and varying with temperature and strain rate as shown in Figure 18, the serration amplitude of dynamic strain aging (at a compressive strain of 0.25) was plotted vs. temperature, for strain rates of 10^{-4}, 10^{-5}, and 10^{-6} sec^{-1} (see Figure 19). Again the interaction displays a peak and the temperature of the peak increases with increasing strain rate.

The drag stress vs. temperature curves of Figure 18, and the serration amplitude vs. temperature curves of Figure 19 can be used to determine an activation energy from the relation $\dot{\varepsilon} = A(e^{-Q}/RT)$ where $\dot{\varepsilon}$ is the strain rate, A is a constant, Q is the activation energy, R is the gas constant, and T is the absolute temperature. In this situation, the structure can be assumed constant. The peak drag stress represents maximum solute-dislocation interaction, therefore, the structure at the peak of each strain rate in Figures 18 and 19 would be one of maximum interaction and would be constant. Plotting log $\dot{\varepsilon}$ vs. 1/T for the temperature of the peak of each strain rate in Figures 18 and 19 results in Figures 20 and 21 respectively. An activation energy, Q, can be obtained from the slope of the line in Figures 20 and 21 and values

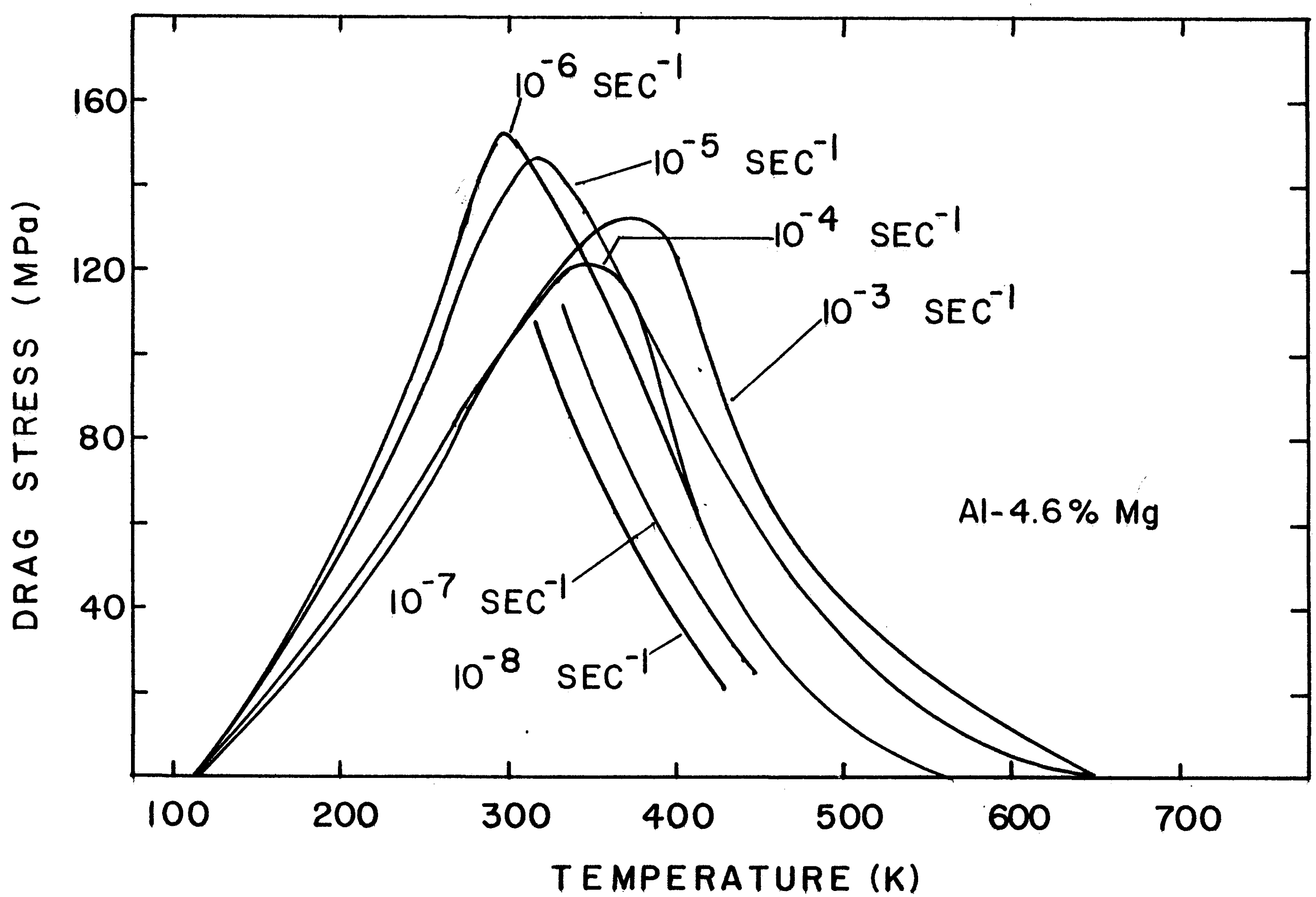

Figure 18 Drag stress-temperature curves showing the variation of drag stress with temperature at different strain rates.

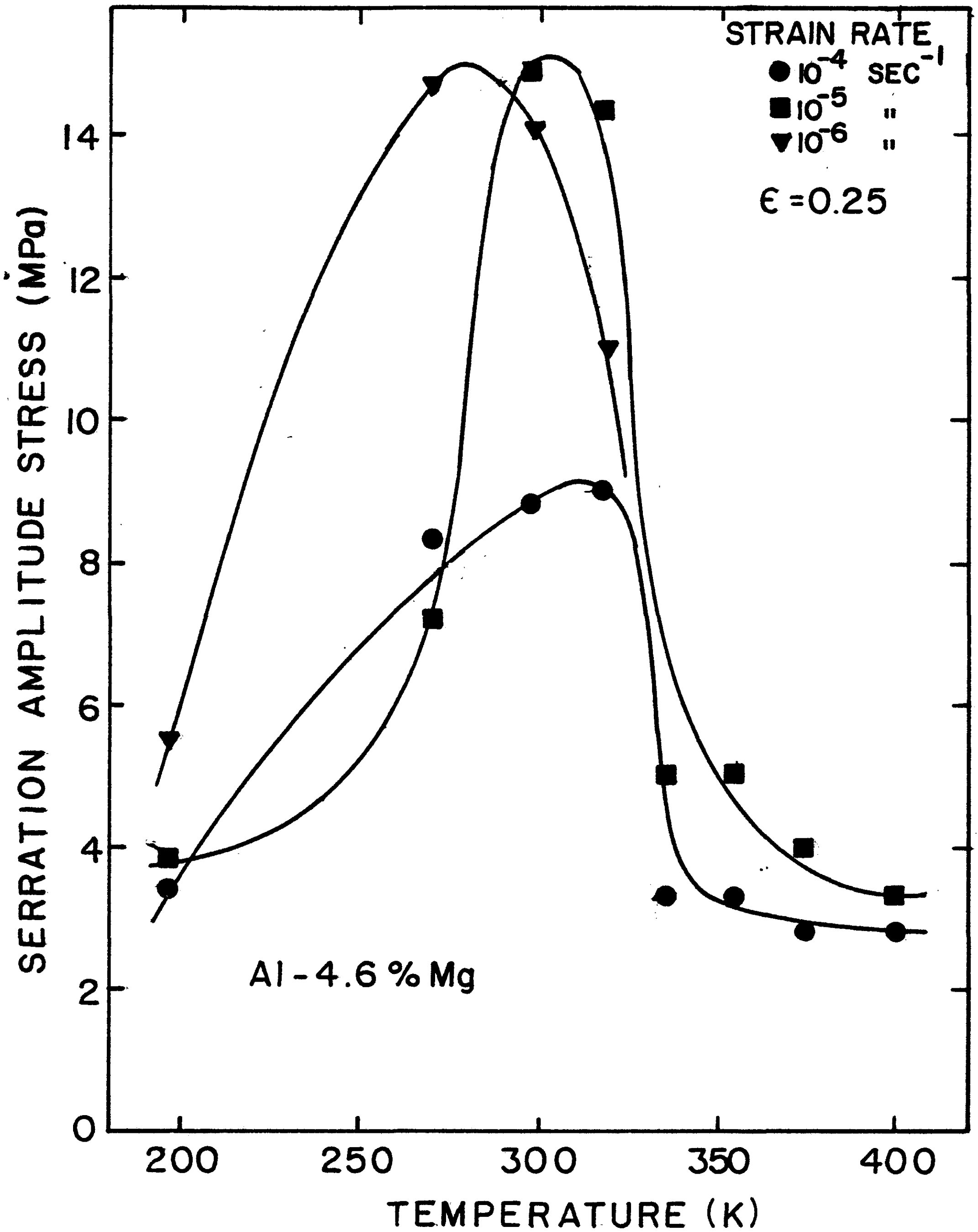

Figure 19 Serration amplitude vs. temperature. The peak in each curve is the temperature of maximum solute-dislocation for that strain rate.

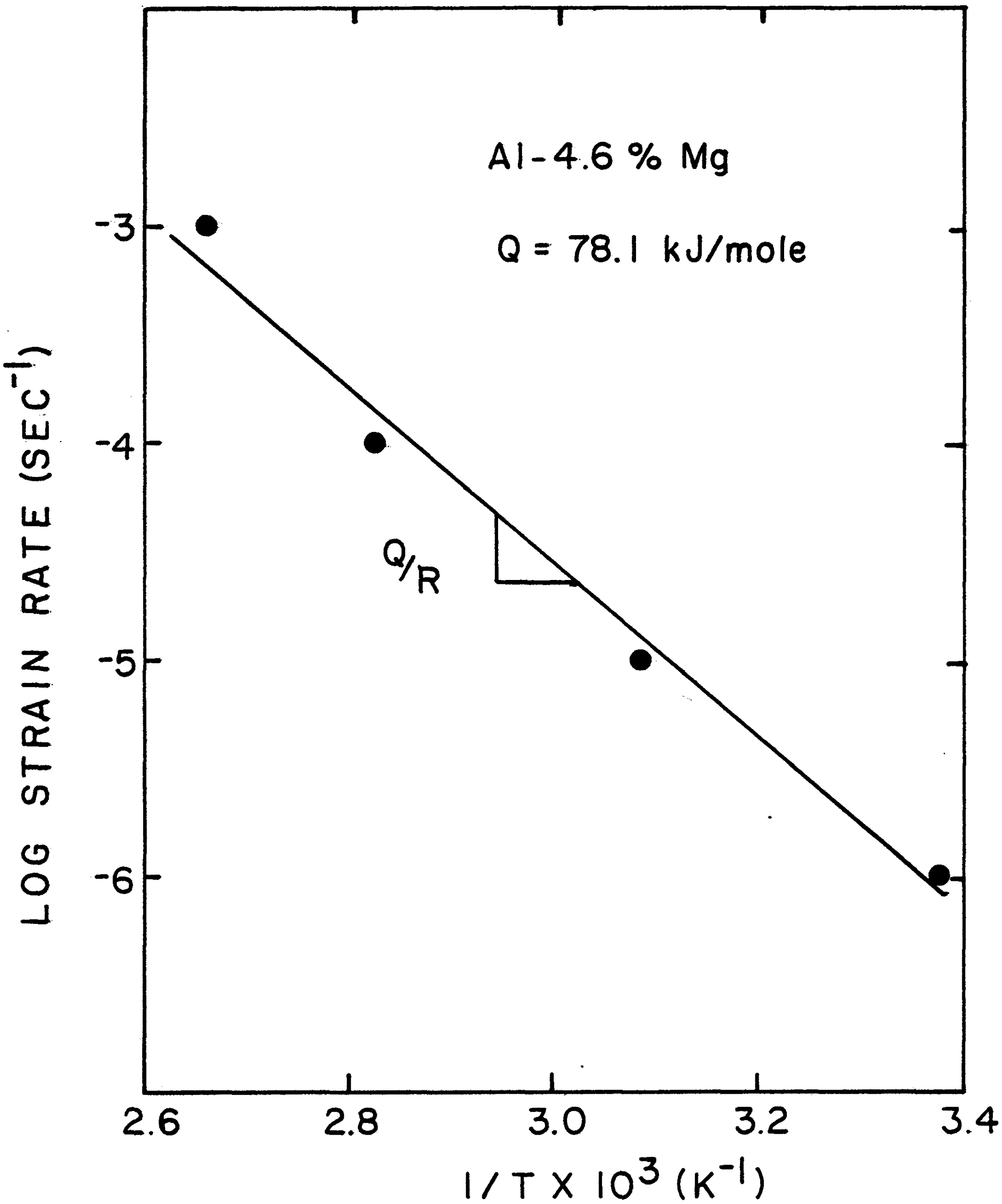

Figure 20 Curve to determine the activation energy of solute-dislocation interaction. The points were generated from the peak of the curves in Figure 18.

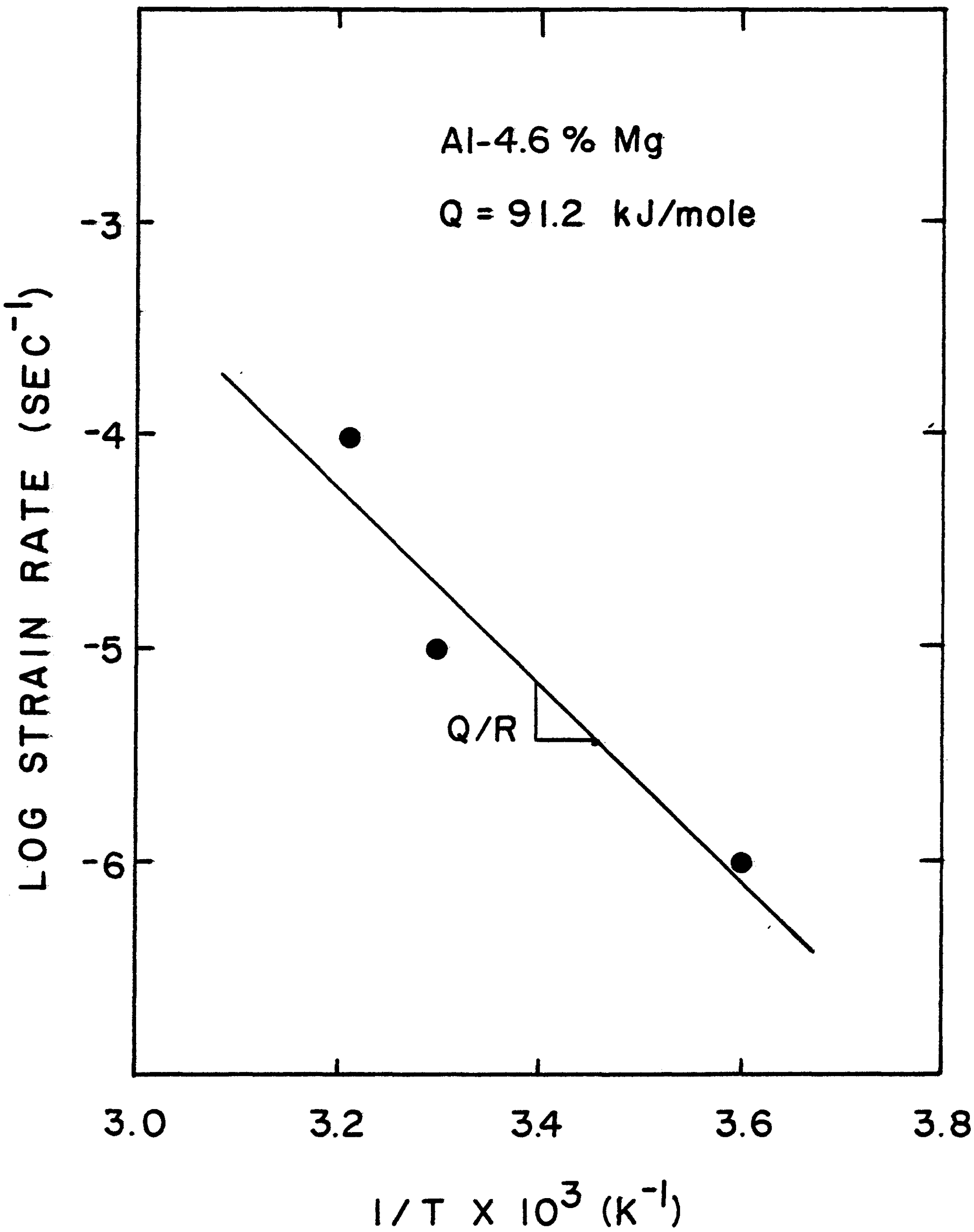

Figure 21 Curve to determine the activation energy of solute-dislocation interaction. The points were generated from the peak of the curves in Figure 19.

of 78.1 and 91.2 kJ/mole were found respectively. The significance of the difference in these values is unclear, but they are both within the range of values determined by other investigators working with the same Al-Mg alloy. For example, Kirk (1977), reported activation energies from 72 kJ/mol for nucleation of Luder's bands during static creep to 81 kJ/mol for nucleation of Luder's bands during cyclic creep. Kirk, Matlock, and Edwards (1978), and Powell (1978), reported activation energies of 73.2 and 95.7 kJ/mol respectively, for the frequency of nucleation of Luder's bands as evidenced by strain bursts during creep tests.

After establishing the empirical relationship between drag stress and temperature at various strain rates (Figure 18) creep tests were performed in an attempt to correlate cyclic creep acceleration with drag stress. Stresses were chosen in an attempt to develop steady state strain rates of 10^{-7} to 10^{-5} sec^{-1}. Figures 22 through 28 are pairs of creep curves run at temperatures ranging from 273 to 485 K. Static and cyclic creep tests were also conducted at 197 K but no measurable creep was seen.

Figure 29 shows the steady state strain rate ratio of cyclic to static creep as a function of temperature. There is an apparent maximum in the creep rate ratio at 338 K. This is precisely what Kirk (1977) found; furthermore, this maximum also coincides with the temperature of maximum solute-dislocation interaction shown by the activation energy curve

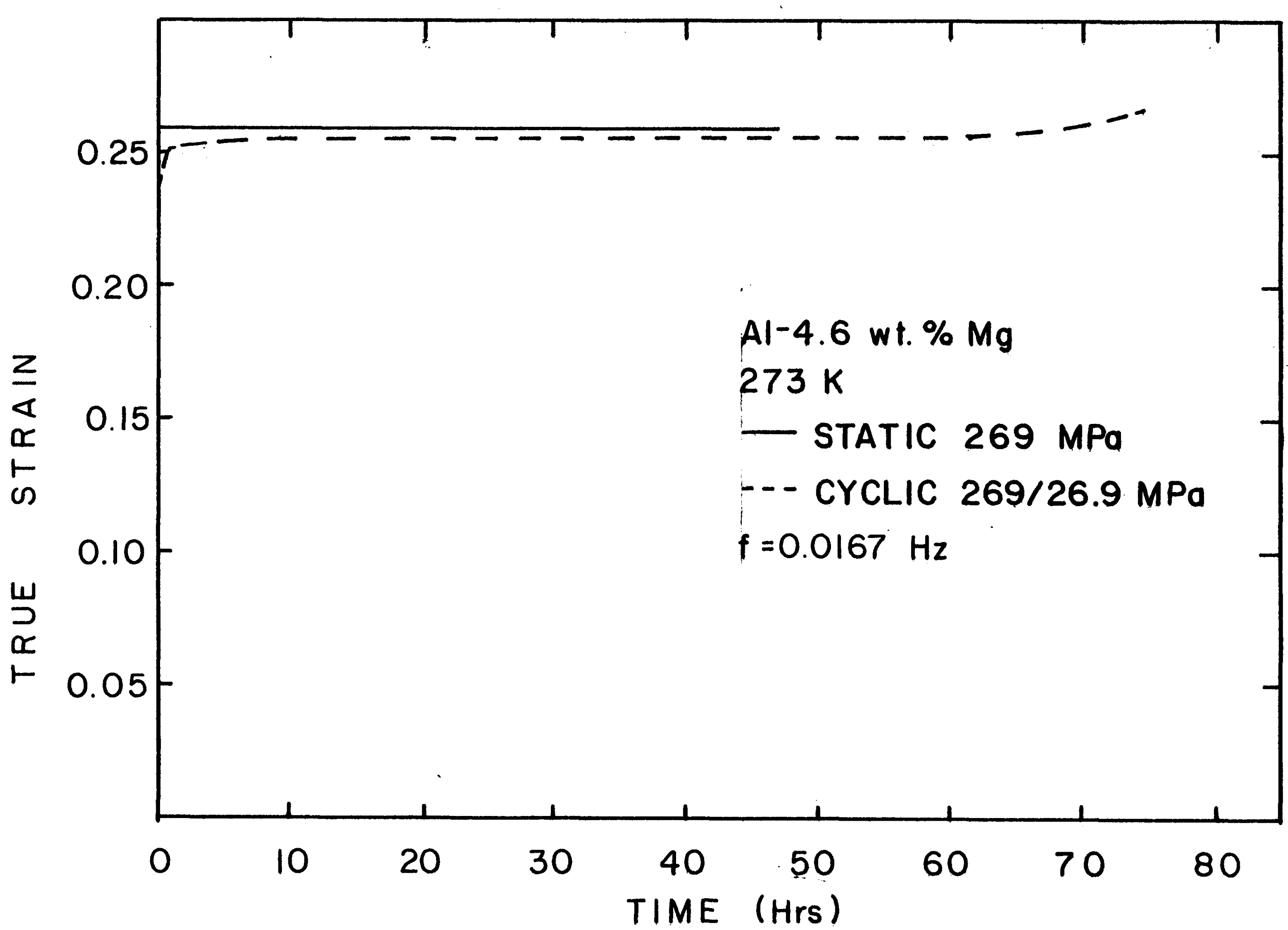

Figure 22 Static and cyclic creep curves of Al-4.6 wt. % Mg at 273 K.

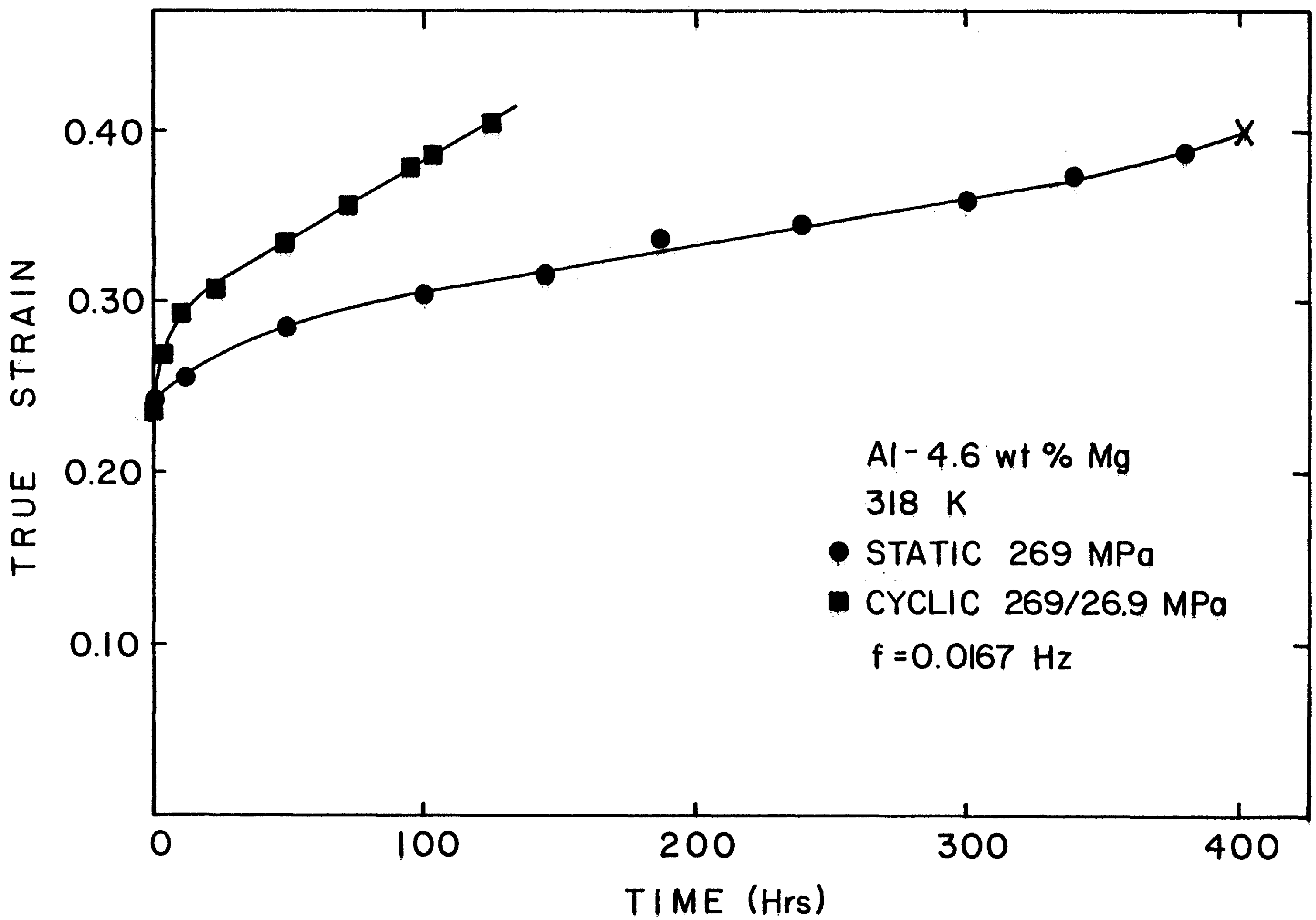

Figure 23 Static and cyclic creep curves of Al-4.6 wt. % Mg at 318 K. Note the accelerated cyclic creep rate.

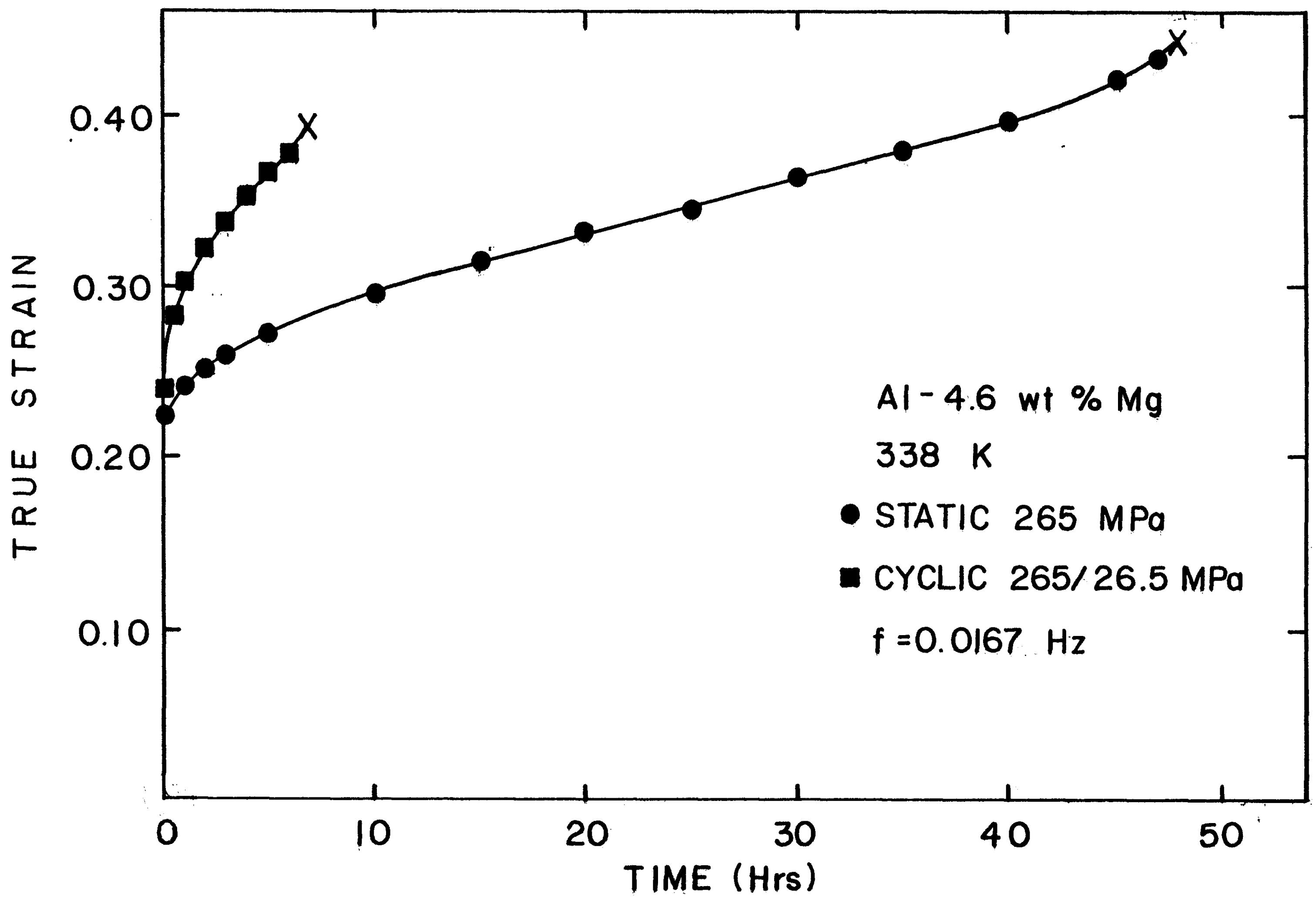

Figure 24 Static and cyclic creep curves of Al-4.6 wt. % Mg at 338 K. Note the accelerated cyclic creep rate.

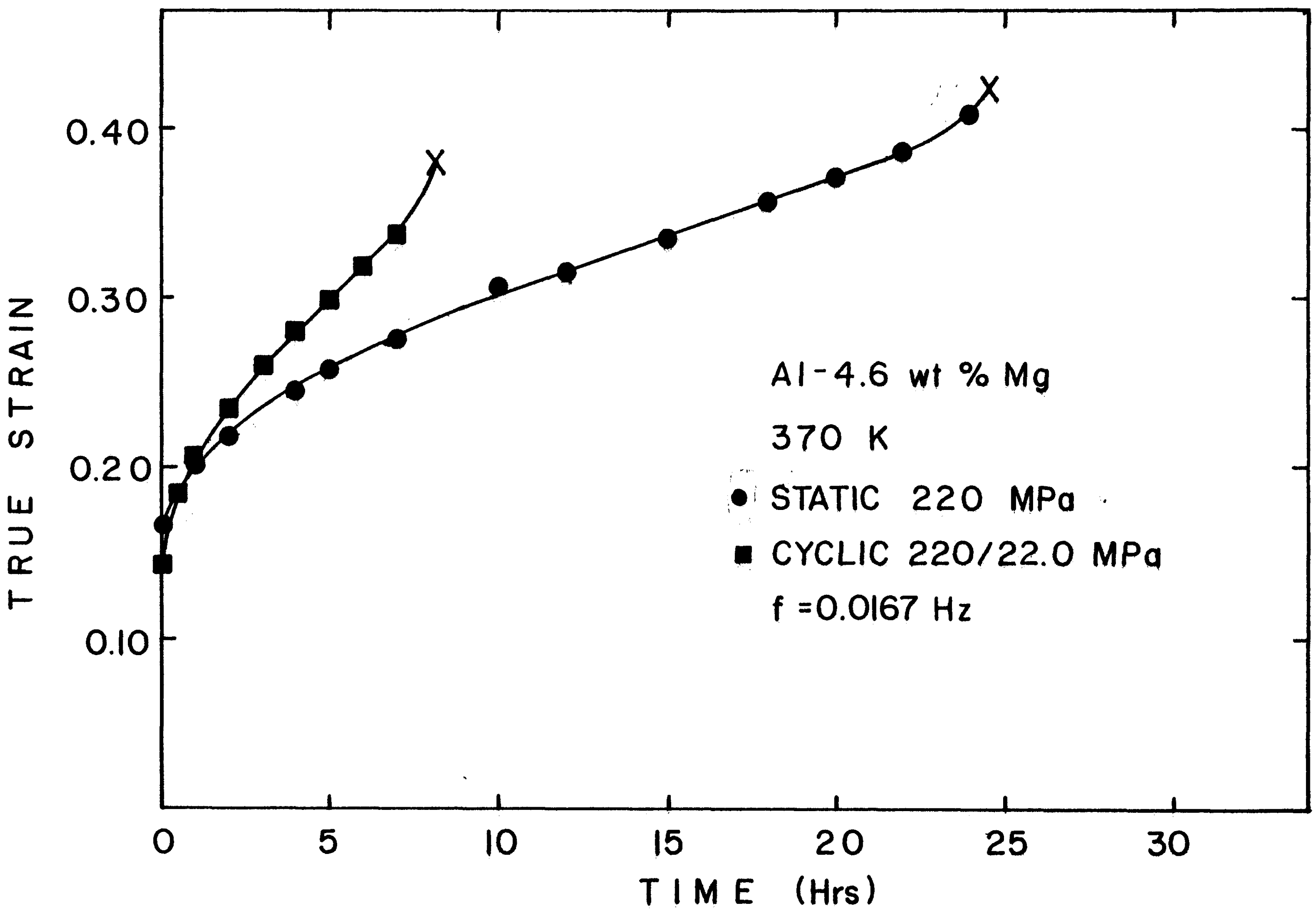

Figure 25 Static and cyclic creep curves of Al-4.6 wt. % Mg at 370 K. Note the accelerated cyclic creep rate.

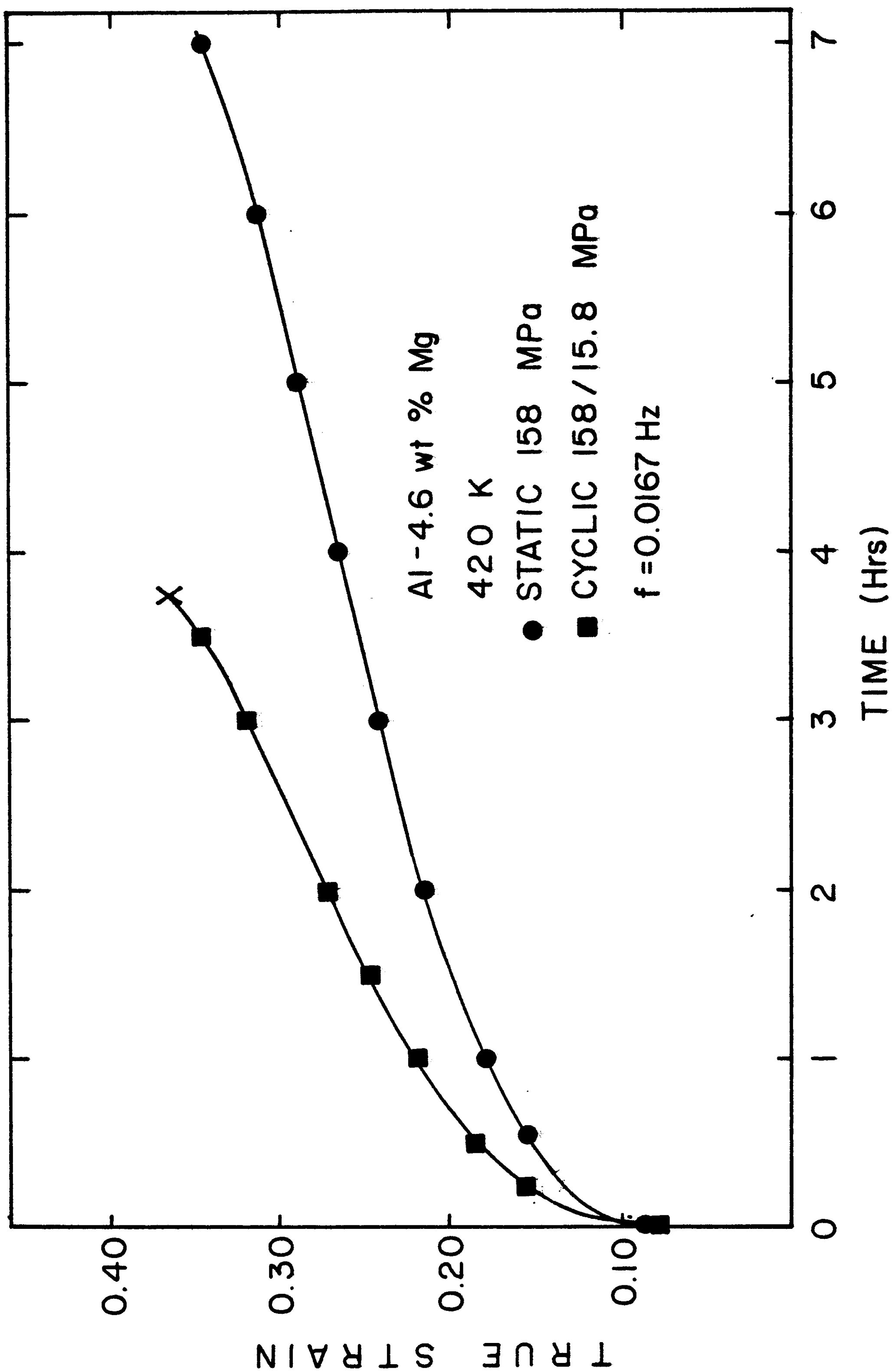

Figure 26. Static and cyclic creep curves of Al-4.6 wt. % Mg at 420 K. Note the accelerated cyclic creep rate.

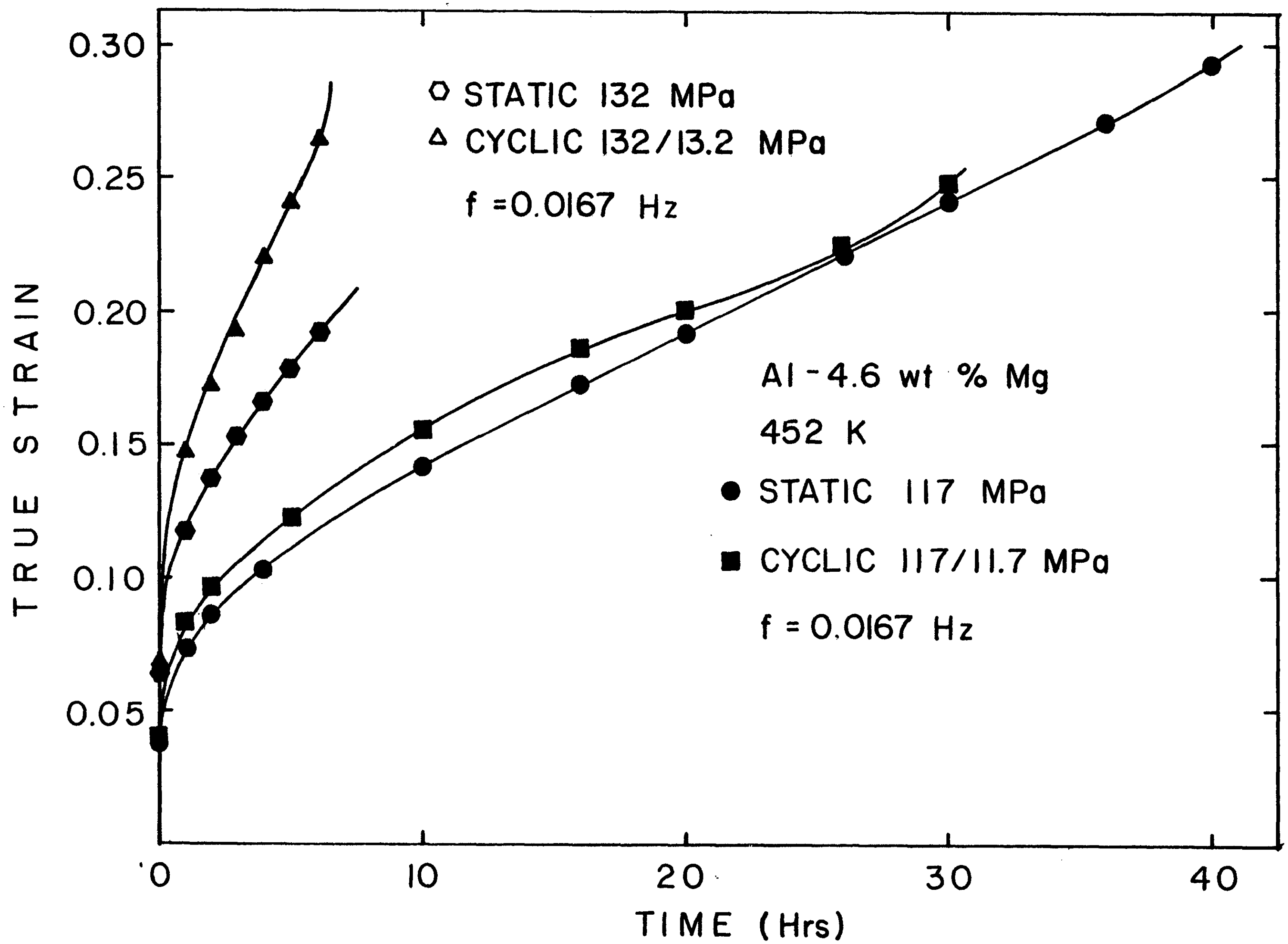

Figure 27 Static and cyclic creep curves of Al-4.6 wt. % Mg at 452 K. and two different stresses. Note the accelerated cyclic creep rate at the high stress but slightly retarded cyclic creep rate at the lower stress.

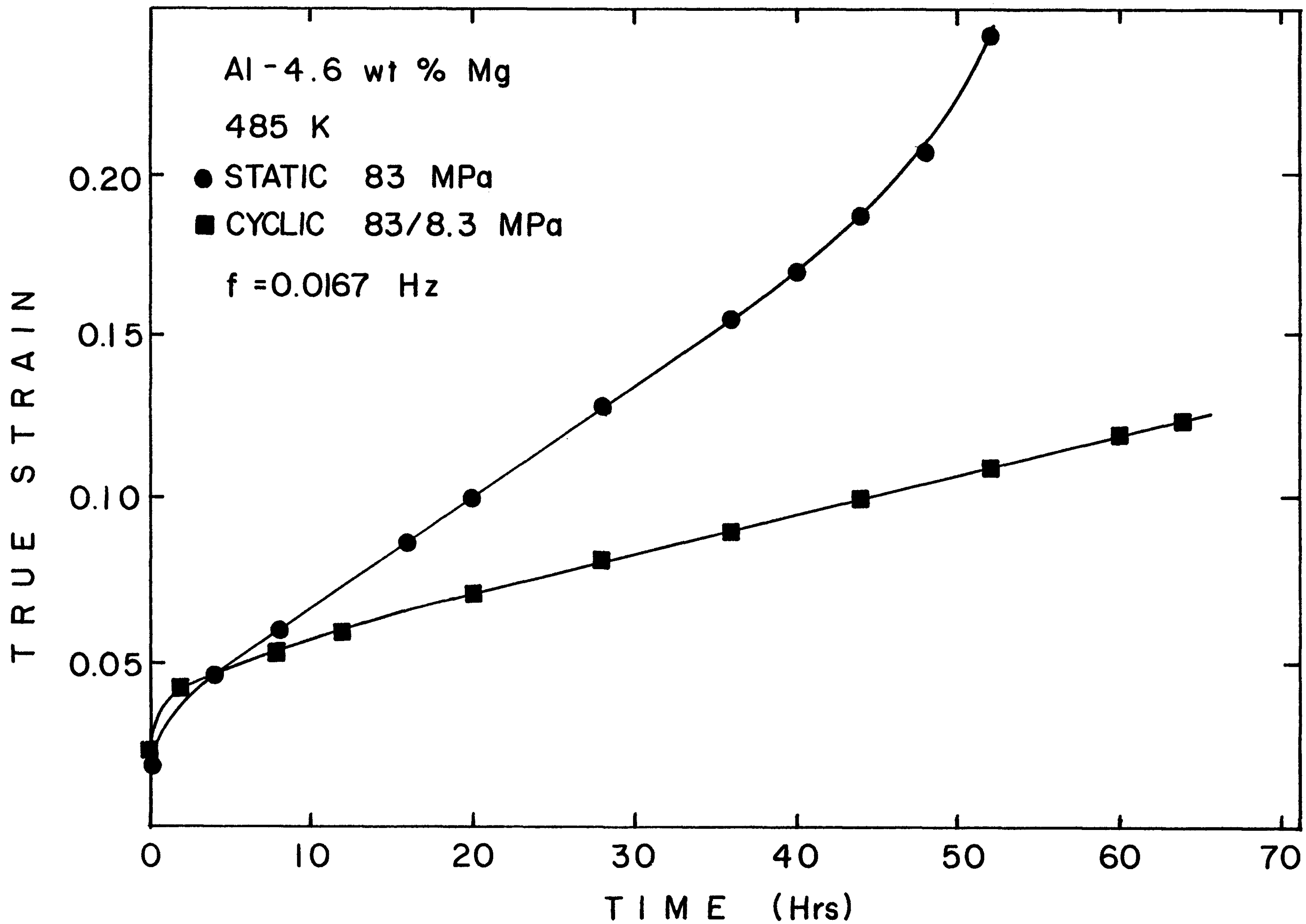

Figure 28 Static and cyclic creep curves of Al-4.6 wt. % Mg at 485 K. Note the greatly retarded cyclic creep rate.

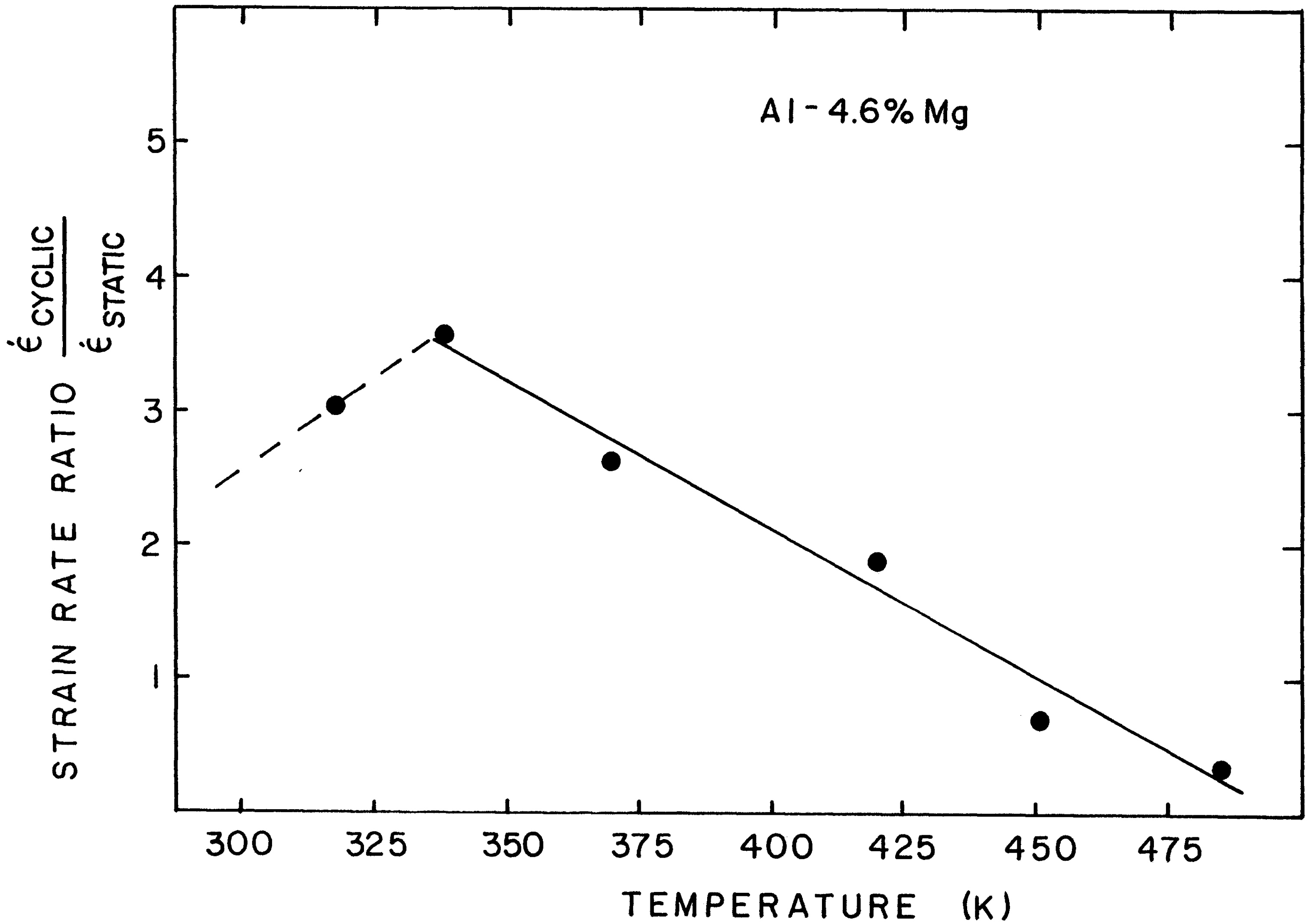

Figure 29 The ratio of cyclic to static creep rates vs. temperature. There is an apparent peak in the cyclic creep acceleration at 338 K.

in Figure 3. If the sum of the drag stress curves of Figure 18 were drawn, the maximum would be centered at approximately 338 K. The implication here is that cyclic creep acceleration is greatest when the drag stress or solute-dislocation interaction is greatest. This is very clearly shown in Figure 30, in which the creep rate ratio, taken from Figure 29, is plotted against the drag stress taken from Figure 18 at constant temperatures. The temperature labeling each point is that of a static and cyclic creep test pair.

To further test the correlation between cyclic creep acceleration and solute-dislocation interactions, the cyclic creep data of Nam (1974), and Powell (1978), working with the same alloy, were plotted in Figure 31. The data generated by Nam (1974) were from tests cycled at frequencies between 0.052 and 0.035 Hz, and a stress amplitude from σ to 0.2σ. Powell (1978) tested his samples at a frequency of 0.027 Hz and a stress amplitude from σ to 0.1σ. The same trend is evident: Cyclic creep acceleration in Al-4.6 wt. % Mg can be correlated directly with the magnitude of the interaction between magnesium solutes and mobile dislocations.

One can see from either Figure 30 or 31 that there appears to be a threshold drag stress or a drag stress where the ratio of cyclic to static creep rates is equal to 1. Drag stresses encountered which are greater than the threshold drag stress cause cyclic creep acceleration and drag stresses smaller than the threshold value permit cyclic creep retardation.

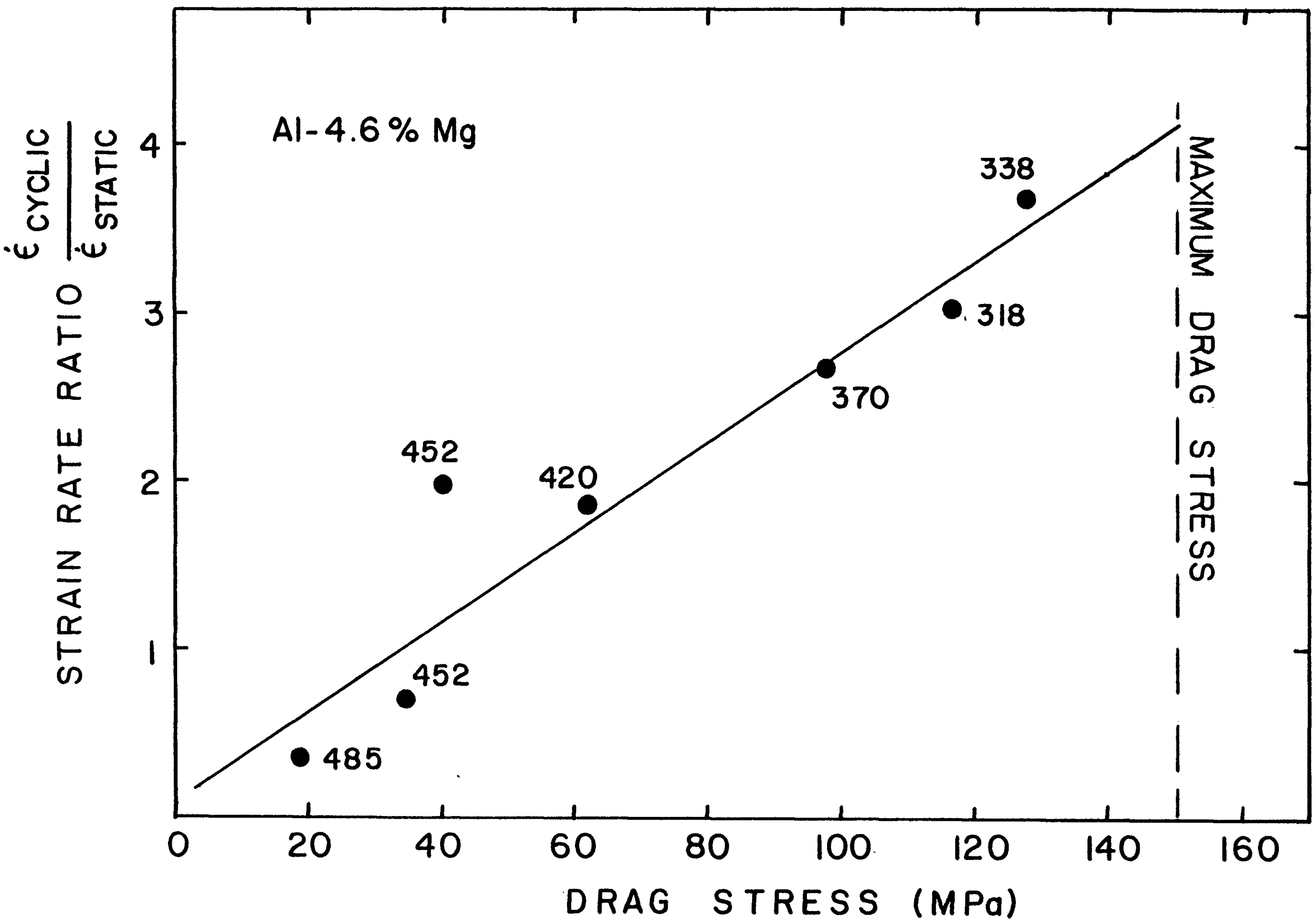

Figure 30 The relationship between creep acceleration and the drag stress or solute-dislocation interaction. The numbers associated with the points are the temperatures (K) of the creep tests.

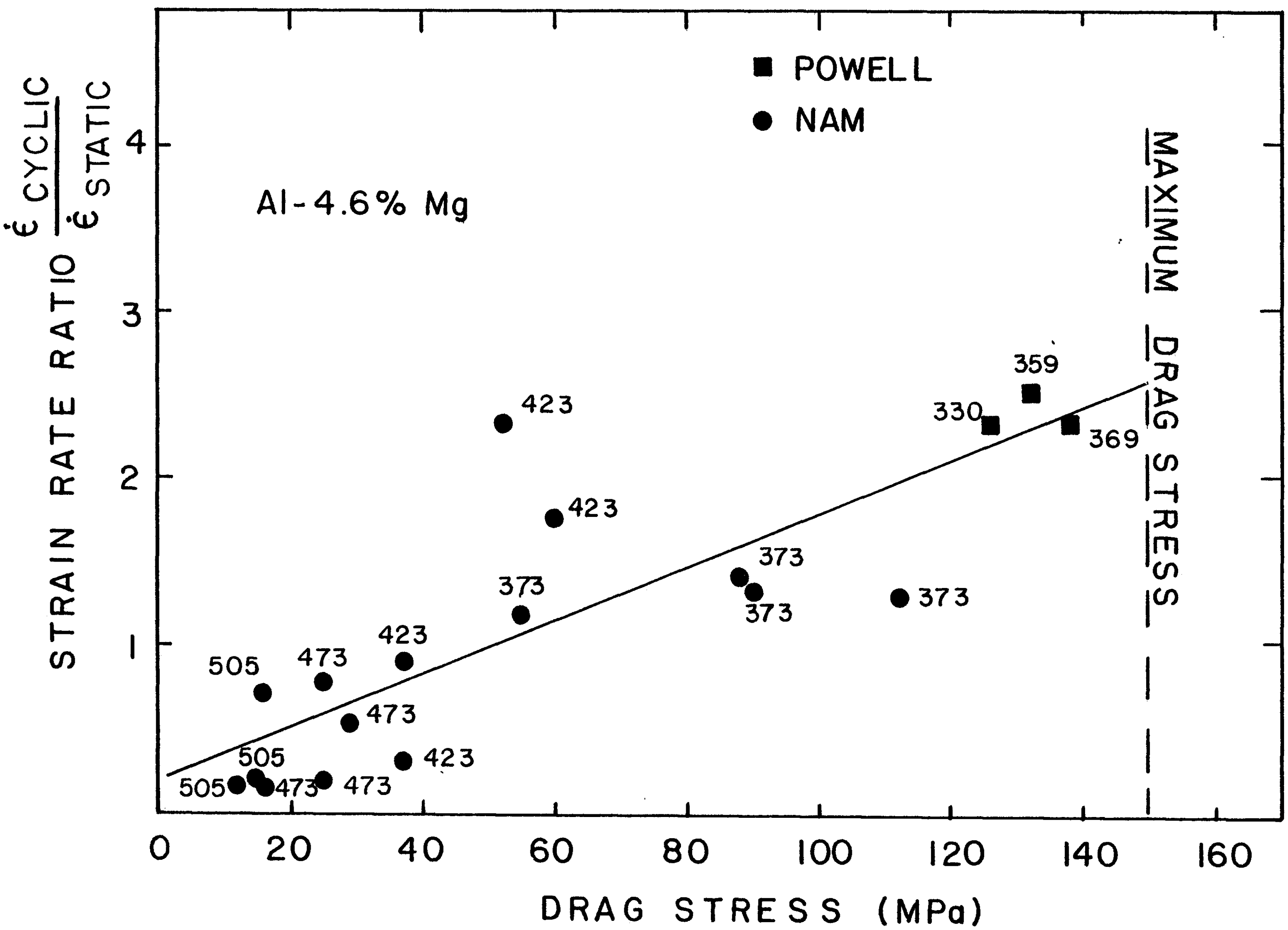

Figure 31 The relationship between creep acceleration and the drag stress from data from Nam, (1974), and Powell, (1978). The numbers indicate the temperature of the creep tests.

While this is apparent, it must be realized that this in no way implies there is a single threshold applied stress which gives the same results. The drag stress can be controlled by appropriate combinations of stress and temperature. If the combination is such that a large drag stress results, the static creep rate will be low. The cyclic creep rate will be accelerated by comparison because stress cycling seems to negate the effects of the solute on dislocation mobility. Nam's data at 423 K and the data presented here at 452 K illustrate this point quite clearly. Table 2 gives the data for the points labeled 423 in Figure 31 and the points labeled 452 in Figure 30. The low stress points have low strain rates and consequently low drag stresses. The solute-dislocation interaction is not strong, and the result is cyclic creep retardation. At the high stresses, the strain rates are high enough to develop larger solute dislocation interactions, which result in large drag stresses and cyclic creep acceleration.

The question to be answered is: Is the cyclic creep rate anomalously high or is the static creep rate anomalously low in the dynamic strain aging range?

A fair and safe answer is that anomalies in both strain rates contribute to their difference. The static strain rate is low because of solute pinning of dislocations. Mobile dislocations become pinned and unavailable for deformation. The pinned dislocations also become obstacles to the motion of other mobile dislocations.

TABLE 2

Cyclic to static creep rate ratios at high and low stresses.

	Temperature (K)	Stress (MPa)	Ratio $\frac{\dot{\varepsilon}\ \text{cyclic}}{\dot{\varepsilon}\ \text{static}}$
Nam, 1974:	423	88.1	0.32
	423	93.7	0.91
	423	114.5	2.34
	423	134.7	1.78
This Investigation:	452	117	0.71
	452	132	1.98

On the other hand, cycling the stress can create a number of situations which aid deformation. If the dislocation density is increased by stress cycling, dislocation pipe diffusion could aid in dislocation climb and permit the circumlocution of obstacles by mobile dislocations, resulting in additional deformation. If cycling causes the injection of mobile dislocations into the system by operating dislocation sources, deformation will be enhanced as a result of the large number of unpinned dislocations. Back and forth motion of jogged screw dislocations by stress cycling could result in a large nonequilibrium concentration of vacancies. These vacancies could aid in dislocation climb around obstacles. They could also permit the motion of dislocations with atmospheres to move by enhancing diffusion of the solute atoms associated with dislocations, thus reducing the solute drag. Back and forth motion of dislocations could also hinder the ability of solute atoms to form atmospheres around dislocations. More mobile dislocations would then be available for deformation.

This investigation accomplished its purpose in clearly revealing the relationship between cyclic stress, creep acceleration and solute-dislocation interaction. Finding the mechanisms responsible for this relationship would be an excellent topic for further research.

CONCLUSIONS

1. There is a direct correlation between the magnitude of solute-dislocation interaction and cyclic creep acceleration.

2. A larger solute-dislocation interaction results in greater acceleration.

3. The activation energies determined for solute-dislocation interactions were similar to those of other investigators.

4. A threshold drag stress was found. Values of drag stress greater than the threshold value caused cyclic creep acceleration. Values of drag stress less than the threshold value resulted in cyclic creep retardation.

LITERATURE CITED

Andrade, E.N. da C., Jolliffe, K.H., 1952. The flow of poly-crystalline metals under simple shears. Proceedings of the Royal Society of London. V. 213A. P.3-26.

Borch, N.R., Shepard, L.A., Dorn, J.E., 1960. Activation energies for creep of a solid solution of magnesium in aluminum. Transactions of the American Society for Metals. V. 52. P. 494-513.

Bradley, W.L., August, J.S., Matlock, D.K., 1977. The effect of grain size on creep rate in pure aluminum at 480 K. Metal Science. V.11. P. 168-170.

Brindley, B.J., Worthington, P.J., 1969. Serrated yielding in Al-3% Mg. Acta Metallurgica. V.17. P. 1357-1361.

Cottrell, A.H., 1953. A note on the Portevin-LeChatelier Effect. Philosophical Magazine. V.44. P. 829-832.

Cottrell, A.H., Jawson, M.A., 1949. Proceedings of the Royal Society. V. A199. P. 104.

Coutinho, C.B., Matlock, D.K., Bradley, W.L., 1975. Cyclic creep of Al-4.6% Mg at moderate temperatures. Materials Science and Engineering. V.21. P.239-247.

Garofalo, F., Richmond, O., Domis, W.F., 1962. Design of apparatus for constant-stress or constant-load creep tests. J. Basic Engr. V. 84. P. 287.

Gibbons, T.B., Herd, H.S., McCartney, L.N., McLean, D., 1973. Creep under varying load. Metal Science Journal. V.7. P. 196-204.

Jakowluk, A., 1970. The influence of various parameters on the process of vibrocreep in metals. Bulletin De L'Academie Polonaise Des Science. V. XVIII. No. 1. P. 7.

Johnston, W.G., Gilman, J.J., 1959. Dislocation velocities, dislocation densities, and plastic flow in lithium fluoride. V. 30. #2. P. 129-144.

Kamel, R., Bessa, F. A., 1971. Effect of superimposed small vibrations on the static creep behavior of polycrystalline zinc. Acta Metallurgica. v. 13. January 1971. p.19.

Kennedy, A. J. 1956. Effect of fatigue stresses on creep and recovery. Proceedings of the International Conference on Fatigue of Metals. London. p. 401.

Kennedy, A. J., 1962. Interactions between creep and fatigue in aluminum and certain of its alloys. Joint Triterm Conference on Creep. p. 3-17.

Kirk, J. L. 1977. Solute effects during cyclic creep. MS Thesis #T1941. Colorado School of Mines.

Kirk, J. L., Matlock, D. K., Edwards, G. R. 1978. Solute effects during static and cyclic creep of Al-4.6 % Mg. To be published.

Kitagawa, M., Jaske, C. E., Morrow, J. 1969. Influence of temperature on reversed creep fatigue at high temperature. ASTM STP 459, American Society for Testing and Materials. p. 100.

Kiyotsugu, O., Marin, J. 1964. Creep of metals under non-steady conditions of stress. Proc. Instn. Mech. Engrs. v. 178 pt 3L. p. 126.

Knause, S. E. 1975. The effect of stress function variations on the fatigue perturbed creep on an Al-Mg alloy. MS Theses #T-1779. Colorado School of Mines.

Koterazawa, R. 1971. A static-to-dynamic transition in creep of metallic materials under cyclic stress conditions. The Fourteenth Japan Congress on Materials Research. March, 1971. p. 73.

MacEwen, S. R., Ramaswami, B. 1970. Dynamic strain aging and jerky flow in Al-Mg single crystals. Philosophical Magazine. v. 22. p. 1025-1037.

Mukherjee, K., D'Antonio, C., Maciay, R., Fischer, G. 1968. Impurity-dislocation interaction and repeated yielding in a commercial Al alloy. Journal of Applied Physics. v. 39. p. 5434-5440.

Nam, S. W. 1974. A phenomenological theory of fatigue-perturbed and normal creep of an Al-4.6%Mg alloy at high temperatures. PhD Thesis #T-1682. Colorado School of Mines.

Powell, J. 1978. Ms Thesis #T-2161. Colorado School of Mines.

Price, A. T. 1967. Creep-fatigue behavior of polycrystalline zinc. Journal of the Institute of Metals. v. 95. p. 87.

Reed-Hill, R. E. 1973. Physical metallurgy principles. D. Van Norstrand Company, New York. p. 341, 345.

Reimann, W. H., Wood, W. A. 1964. Room temperature creep in iron under tensile stress and superposed alternating torsion. Trans AIME. v. 230. p. 1327.

Rising, T. 1978. PhD Thesis #T-2105. Colorado School of Mines.

Scheffler, K.D. 1972. Interactions between creep fatigue and strain aging in two refractory metal alloys. Met Trans. v. 3. p. 167

Sheldon, G. P., Yeske, R. A. 1978. Effects of oxygen concentration and temperature on cyclic creep in niobium-oxygen alloys. Met Trans. v. 9A. p. 5.

Shetty, D. K., Meshii, M. 1975. Plastic deformation of aluminum under repeated loading. Met Trans. v. 6A. p. 349.

Shetty, D. K., Meshii, M. 1977. Influence of carbon on the static and cyclic creep behavior of alpha iron. Materials Science and Engineering. v. 32. p. 283.

Sherby, O. D., Anderson, R. A., Dorn, J. E. 1951. Effect of alloying elements on the elevated temperature plastic properties of alpha solid solutions of aluminum. Journal of Metals. v. 3. p. 643.

Sherby, O. D., Burke, P. M. 1968. Mechanical behavior of crystalline solids at elevated temperatures. Progress in Material Science. v. 13. p. 325.

APPENDIX I

The curve used in designing the lever arm of the constant stress creep apparatus was generated by the two equations given in Chapter II. A short computer program was used to generate points which were then plotted, full scale on an X-Y plotter and connected by a smooth curve. The plotted curve then became a template for cutting the lever arm out of one inch thick aluminum plate. The arm pivoted on a four inch knife and was balanced using adjustable counter weights which can be seen in Figure 5. Since the grip assembly was suspended from a constant radius it was also counter balanced with a weight hanging from a constant radius. This also can be seen in Figure 5. The weight of the weight pan assembly was known and was included in the total load to achieve the desired stress.

Constant stress accuracy was checked using a load cell in the position of a sample and a linear variable differential transformer (LVDT) to measure displacement. Constant stress was found to vary by the acceptable amount of 0.5%.

The frame of the creep apparatus was bolted to the floor and wall to eliminate vibrations due to cycling. The pneumatic cycling system was not connected to the frame for the same reason.

APPENDIX II

Presented in Appendix II are data from compression tests. Data were taken at four true strains, 0.10, 0.15, 0.20 and 0.25. In the tables, σ refers to the true stress. When serrated yielding was seen the maximum true stress, the minimum true stress and the stress amplitude for each true strain value are represented as σHigh, σLow and $\Delta\sigma$ respectively. Tests were conducted at nominal strain rates of 10^{-3}, 10^{-4}, 10^{-5} and 10^{-6} sec^{-1}. The actual true strain rates are given in the row labeled $\dot{\varepsilon}$ with the number in parentheses indicating the order of magnitude.

197 K

		TRUE STRAIN			
		0.10	0.15	0.20	0.25
	$10^{-3}sec^{-1}$				
σ High	psi	33120	38070	41440	44160
	MPa	228	262	286	304
σ Low	psi				
	MPa				
Δσ	psi				
	MPa				
	$\dot{\varepsilon}$ (10^{-3})	1.114	1.171	1.231	1.294
	$10^{-4}sec^{-1}$				
σ High	psi	33590	38070	41330	43940
	MPa	231	262	285	303
σ Low	psi	33110	37610	40810	43450
	MPa	228	259	281	299
Δσ	psi	480	460	520	495
	MPa	3.3	3.2	3.6	3.4
	$\dot{\varepsilon}$ (10^{-4})	1.038	1.091	1.147	1.206
	$10^{-5}sec^{-1}$				
σ High	psi	33680	38200	41360	43960
	MPa	232	263	285	303
σ Low	psi	33220	27670	40940	43410
	MPa	229	260	282	299
Δσ	psi	460	530	420	560
	MPa	3.2	3.7	2.9	3.8
	$\dot{\varepsilon}$ (10^{-5})	0.9489	0.9976	1.049	1.102

197 K

(Continued)

		0.10	0.15	0.20	0.25
10^{-6} sec^{-1}					
σ High	psi	32980	37470	39930	43420
	MPa	227	258	275	299
σ Low	psi	32330	36590	39170	42620
	MPa	223	252	270	294
$\Delta\sigma$	psi	650	880	760	800
	MPa	4.5	6.1	5.2	5.5
	$\dot{\varepsilon}$ (10^{-6})	0.9329	0.9807	1.031	1.084

271 K

		TRUE STRAIN			
		0.1	0.15	0.20	0.25
$10^{-3}\,sec^{-1}$					
σ High	psi	32940	37150	40190	42610
	MPa	227	256	277	294
σ Low	psi				
	MPa				
Δσ	psi				
	MPa				
$\dot{\varepsilon}$	(10^{-3})	1.140	1.198	1.260	1.324
$10^{-4}\,sec^{-1}$					
σ High	psi	32700	37210	40440	42940
	MPa	225	256	279	296
σ Low	psi	31590	36150	39170	41740
	MPa	218	249	270	288
Δσ	psi	1110	1060	1270	1200
	MPa	7.6	7.3	8.8	8.3
$\dot{\varepsilon}$	(10^{-4})	1.106	1.163	1.222	1.285
$10^{-5}\,sec^{-1}$					
σ High	psi	32980	38090	42030	44540
	MPa	227	262	290	307
σ Low	psi	31960	36940	40690	43500
	MPa	220	254	280	300
Δσ	psi	1020	1150	1340	2130
	MPa	7.0	7.9	9.2	7.2
$\dot{\varepsilon}$	(10^{-5})	1.136	1.194	1.255	1.320
$10^{-6}\,sec^{-1}$					
σ High	psi	32650	37780	41500	44530
	MPa	225	260	286	307
σ Low	psi	31370	36470	39840	42400
	MPa	216	251	274	292
Δσ	psi	1280	1310	1660	2130
	MPa	8.8	9.0	11.4	14.7
$\dot{\varepsilon}$	(10^{-6})	1.123	1.180	1.241	1.305

		TRUE STRAIN			
		0.1	0.15	0.20	0.25
$10^{-3}sec^{-1}$					
σ High	psi	32240	36760	39930	42460
	MPa	222	253	275	293
σ Low	psi	31770	36320	39510	41980
	MPa	219	250	272	289
Δσ	psi	470	440	420	480
	MPa	3.2	3.0	2.9	3.3
$\dot{\varepsilon}$	(10^{-3})	1.075	1.130	1.188	1.249
$10^{-4}sec^{-1}$					
σ High	psi	32520	37350	40710	43340
	MPa	224	257	280	299
σ Low	psi	31320	36030	39290	42070
	MPa	216	248	271	290
Δσ	psi	1200	1320	1420	1270
	MPa	8.3	9.1	9.8	8.8
$\dot{\varepsilon}$	(10^{-4})	1.075	1.130	1.188	1.249
$10^{-5}sec^{-1}$					
σ High	psi	32850	37760	41030	43810
	MPa	226	260	283	302
σ Low	psi	31280	36180	39190	41650
	MPa	216	249	270	287
Δσ	psi	1570	1580	1840	2160
	MPa	10.8	10.9	12.7	14.9
$\dot{\varepsilon}$	(10^{-5})	1.092	1.148	1.207	1.268
$10^{-6}sec^{-1}$					
σ High	psi	32380	37660	41510	44440
	MPa	223	259	286	306.2
σ Low	psi	31380	36090	39860	42400
	MPa	216	249	275	292
Δσ	psi	1000	1570	1650	2040
	MPa	6.9	10.8	11.4	14.1
$\dot{\varepsilon}$	(10^{-6})	1.109	1.166	1.225	1.288

		TRUE STRAIN			
		0.10	0.15	0.20	0.25
$10^{-3}sec^{-1}$					
σ High	psi	32500	36790	39830	42160
	MPa	224	253	274	290
σ Low	psi				
	MPa				
Δσ	psi				
	MPa				
$\dot{\varepsilon}$ (10^{-3})		1.088	1.144	1.203	1.265
$10^{-4}sec^{-1}$					
σ High	psi	32580	36980	40310	42830
	MPa	224	255	278	295
σ Low	psi	31860	36040	39090	41520
	MPa	220	248	269	286
Δσ	psi	720	940	1220	1310
	MPa	5.0	6.5	8.4	9.0
$\dot{\varepsilon}$ (10^{-4})		1.080	1.135	1.194	1.255
$10^{-5}sec^{-1}$					
σ High	psi	32520	37210	40600	43340
	MPa	224	256	280	299
σ Low	psi	31220	35790	39090	41260
	MPa	215	247	269	284
Δσ	psi	1300	1420	1510	2080
	MPa	9.0	9.8	10.4	14.3
$\dot{\varepsilon}$ (10^{-5})		1.087	1.443	1.201	1.263
$10^{-3}sec^{-1}$					
σ High	psi	32150	34800	38120	40950
	MPa	221	240	263	282
σ Low	psi	30860	33480	36700	39360
	MPa	213	231	253	271
Δσ	psi	1290	1320	1.420	1590
	MPa	8.9	9.1	9.8	11.0
$\dot{\varepsilon}$ (10^{-6})		1.141	1.200	1.261	1.326

336 K

		TRUE STRAIN			
		0.10	0.15	0.20	0.25
	$10^{-3}sec^{-1}$				
σ High	psi	32340	36470	39460	41750
	MPa	223	251	272	288
σ Low	psi				
	MPa				
Δσ	psi				
	MPa				
	$\dot{\varepsilon}$ (10^{-3})	1.094	1.150	1.209	1.271
	$10^{-4}sec^{-1}$				
σ High	psi	31920	36530	39770	42450
	MPa	220	252	274	292
σ Low	psi	31550	36090	39350	41970
	MPa	217	249	271	289
Δσ	psi	370	440	420	480
	MPa	2.5	3.0	2.9	3.3
	$\dot{\varepsilon}$ (10^{-4})	1.110	1.167	1.226	1.289
	$10^{-5}sec^{-1}$				
σ High	psi	31180	35560	38850	41340
	MPa	215	245	268	285
σ Low	psi	30540	34770	38010	40620
	MPa	210	240	262	280
Δσ	psi	640	790	840	720
	MPa	4.4	5.4	5.8	5.0
	$\dot{\varepsilon}$ (10^{-5})	1.097	1.153	1.212	1.274

355 K

		TRUE STRAIN 0.10	0.15	0.20	0.25
10^{-3}sec^{-1}					
σ High	psi	32520	36500	39430	41660
	MPa	224	252	272	287
σ Low	psi				
	MPa				
Δσ	psi				
	MPa				
	$\dot{\varepsilon}$ (10^{-3})	1.090	1.145	1.204	1.266
10^{-4}sec^{-1}					
σ High	psi	31450	36010	38970	41320
	MPa	217	248	268	285
σ Low	psi	30810	35660	38640	40840
	MPa	212	246	266	281
Δσ	psi	640	350	330	480
	MPa	4.4	2.4	2.3	3.3
	$\dot{\varepsilon}$ (10^{-4})	1.096	1.152	1.211	1.273
10^{-5}sec^{-1}					
σ High	psi	30010	33490	36150	38300
	MPa	207	231	249	264
σ Low	psi	29360	32880	35560	37580
	MPa	202	227	245	259
Δσ	psi	650	610	590	720
	MPa	4.5	4.2	4.1	5.0
	$\dot{\varepsilon}$ (10^{-5})	1.084	1.139	1.197	1.259

375 K

		TRUE STRAIN			
		0.10	0.15	0.20	0.25
	$10^{-3} sec^{-1}$				
σ High	psi	31780	35500	38040	40240
	MPa	219	245	262	277
σ Low	psi				
	MPa				
Δσ	psi				
	MPa				
	$\dot{\varepsilon}$ (10^{-3})	1.122	1.179	1.240	1.303
	$10^{-4} sec^{-1}$				
σ High	psi	30410	33580	35860	37680
	MPa	209	231	247	260
σ Low	psi	24950	33140	35440	37280
	MPa	206	228	244	257
Δσ	psi	460	440	420	400
	MPa	3.2	3.0	2.9	2.8
	$\dot{\varepsilon}$ (10^{-4})	1.099	1.156	1.215	1.277
	$10^{-5} sec^{-1}$				
σ High	psi	27830	30080	31540	32870
	MPa	192	207	217	227
σ Low	psi	27370	29550	31120	32310
	MPa	189	204	214	223
Δσ	psi	460	530	420	560
	MPa	3.2	3.7	2.9	3.9
	$\dot{\varepsilon}$ (10^{-5})	1.091	1.147	1.206	1.268

400 K

		TRUE STRAIN			
		0.10	0.15	0.20	0.25
	$10^{-3}sec^{-1}$				
σ High	psi	30050	33010	35190	36920
	MPa	207	227	242	254
σ Low	psi				
	MPa				
$\Delta\sigma$	psi				
	MPa				
	$\dot{\varepsilon}$ (10^{-3})	1.114	1.171	1.231	1.295
	$10^{-4}sec^{-1}$				
σ High	psi	28020	30250	32020	33320
	MPa	193	208	221	230
σ Low	psi	27650	29900	31610	32920
	MPa	190	206	218	227
$\Delta\sigma$	psi	370	350	410	400
	MPa	2.5	2.4	2.8	2.8
	$\dot{\varepsilon}$ (10^{-4})	1.097	1.153	1.212	1.275
	$10^{-5}sec^{-1}$				
σ High	psi	24880	26300	27350	28320
	MPa	171	181	188	195
σ Low	psi	24330	25780	26850	27840
	MPa	168	178	185	192
$\Delta\sigma$	psi	550	520	500	480
	MPa	3.8	3.6	3.4	3.3
	$\dot{\varepsilon}$ (10^{-5})	1.089	1.145	1.204	1.266